Università Politecnica delle Marche
Scuola di Dottorato di Ricerca in Agraria
Curriculum in Dipartimento di Scienze Agrarie, Alimentari ed Ambientali

---

Remote sensing approaches in Carbon Stock (CS) mapping considering the dominant tree species in urban areas

Ph.D. Dissertation of:

Md Abdul Mueed Choudhury

Advisor:

Prof. Andrea Galli

Curriculum supervisor:

Prof. Ernesto Marcheggiani

Prof. Carlo Urbinati

Università Politecnica delle Marche
Scuola di Dottorato di Ricerca in Agraria
Curriculum in Dipartimento di Scienze Agrarie, Alimentari ed Ambientali

---

Tecniche di Telerilevamento per la Mappatura dello Stock di Carbonio (CS) in aree Urbane in relazione alle specie arbore dominanti

Ph.D. Dissertation of:

Md Abdul Mueed Choudhury

Advisor:

Prof. Andrea Galli

Curriculum supervisor:

Prof. Ernesto Marcheggiani

Prof. Carlo Urbinati

Università Politecnica delle Marche
Dipartimento di (nome del dipartimento dove la tesi e' stata sviluppata)
Via Brecce Bianche — 60131 - Ancona, Italy

Acknowledgements

I wish to thank ...

Abstract

Recently, severe intensification of atmospheric carbon recognizes the importance of urban tree contributions in atmospheric carbon mitigation in city areas considering a sustainable urban green planning and management system. Explicit and timely information on urban trees and their roles in atmospheric Carbon Stock (CS) are essential for the policymakers to take immediate actions to recover the effects of deforestation and their worsening outcomes. This doctoral study will be a way out for the policymakers in CS mapping for the dominant tree species in their cities based on Remote Sensing (RS) data sources. The mapping approach could be a useful tool especially for developing countries, where hyperspectral data could be a better solution over the hardly available LiDAR data. In this study, a detailed methodology on the urban tree CS calibration and mapping was done for two urban areas one of which was in Sassuolo (MO), a smaller city in Italy. The other one was conducted in the capital region of Belgium (Brussels), where also the comparative analysis of the two different remote sensing data sources (LiDAR and WorldView 3 (WV3)) and their mapping outcomes were assessed to define the convenience and applicability of the data sources. In Sassuolo, CS mapping was done utilizing only the WV3 image data for a smaller study area of 22 plots (10m×10m each) where the 7 plots were utilized to validate the results of tree species classification and the CS calibration and mapping. Later in Brussels, the approach was implied for a larger study area of 75 plots (10m×10m each) where 20 plots were utilized for the validation of CS calibration and mapping outcomes. In all cases, either in Sassuolo or in Brussels, dominant tree species were identified and classified utilizing the high-resolution WV3 image. The Object-Based Image Analysis (OBIA) classification approach was successfully employed to attain the overall accuracy of 78% and 71% for the tree species in Sassuolo and Brussels respectively. The field estimations of CS for each plot were done utilizing an allometric model based on the field data on tree dendrometry i.e. Height (H) and Diameter at Breast Height (DBH). Later the computed CS based on the field data along with the WV3 (NDVI) and LiDAR (CHM) data derived variables, had been mapped in QGIS. The results were found quite evident for both cities which did approve the approach as an efficient and convenient way of mapping, certainly recognizing the dominant tree species contributions in atmospheric CS. No doubt, this study will assist the city planners to understand and decide the applicability of remote sensing data sources based on their availability and the level of expediency, ensuring a sustainable urban green management system.

(ITALIAN)
Recentemente, Negli ultimi anni, il preoccupante incremento del contributo del carbonio atmosferico al cambio climatico ha sollevato con forza il dibattito. In area urbana, le misure di mitigazione si stanno concentrando, tra le altre, sul ruolo delle infrastrutture verdi. In particolare, gli approcci improntati a sistemi di pianificazione e gestione del verde urbano sostenibili sembrano essere promettenti. Informazioni esplicite e tempestive sulla composizione strutturale e funzionale delle infrastrutture verdi e sulle singole strutture o aggregati di alberi urbani, in merito al loro ruolo nella cattura del carbonio atmosferico

(CS), sono essenziali affinché i responsabili delle amministrazioni locali adottino azioni immediate per mitigare il peggioramento dell'impatto delle attività antropiche.
In questo studio, è stata adottata una metodologia dettagliata per la calibrazione e mappatura del CS delle alberature in due aree urbane. Uno studio è stato condotto a Sassuolo (MO), una città italiana di dimensioni medie. L'altro, è stato condotto nella regione della capitale del Belgio (Bruxelles), dove sono state anche valutate ed analizzate in modo comparativo le due diverse fonti di dati di telerilevamento (LiDAR e WorldView 3 (WV3)) ed i rispettivi risultati di mappatura. A Sassuolo, la mappatura del CS è stata eseguita utilizzando solo dati da immagini WV3 per un'area di studio alla scala locale di dettaglio. In particolare, alla scala di parco urbano, sono state selezionate 22 parcelle (10 m × 10 m ciascuna) di cui 7 per la validazione dei risultati della classificazione delle specie arboree e della calibrazione e mappatura del CS. In un secondo esperimento, a Bruxelles, l'approccio è stato replicato per un'area di studio più ampia, alla scala di città metropolitana. In questo caso, 75 parcelle (10 m × 10 m ciascuna) sono state utilizzate, di cui 20 per la convalida della calibrazione dei risultati della mappatura del CS. In entrambi i casi, sia a Sassuolo sia a Bruxelles, le specie arboree dominanti sono state identificate e classificate utilizzando immagini WV3 ad alta risoluzione. L'approccio di classificazione OBIA (Object-Based Image Analysis) è stato impiegato con successo ottenendo una precisione complessiva (Overall Accuracy) del 78% e del 71%, rispettivamente, per le relative specie arboree. Le stime del CS per ciascun caso sono state computate, a livello del singolo plot, utilizzando un modello allometrico basato su dati dendrometrici rilevati in campo, ad esempio altezza della pianta (H) e diametro del fusto all'altezza del petto (DBH). Successivamente il CS calcolato in base ai dati dicampo, insieme alle variabili derivate dall'elaborazione dei dati WV3 (NDVI) e LiDAR (CHM), sono stati mappati usando il sistema informativo geografico QGIS. I risultati ottenuti per entrambe le città hanno permesso di validare l'approccio, quale metodo efficiente e conveniente per mappare alla scala urbana, sia media che metropolitana, il contributo delle specie arboree dominanti nella cattura del carbonio atmosferico (CS). Questo studio aiuterà sicuramente urbanisti e pianificatori a meglio comprendere e meglio progettare la pianificazione delle infrastrutture verdi urbane, basandosi su dati provenienti da fonti telerilevate da remoto, e ove possibile prossimali, in base alla loro disponibilità ed al livello di opportunità, al fine di implementare un sistema sostenibile di gestione del verde urbano.

Contents

List of Figures

List of Tables

Chapter 1.

Introduction

In recent decades, ceaseless urbanization and intensifying global warming have led to increased levels of atmospheric carbon in urban areas. For city planners and researchers, understanding the contribution of trees in mitigating atmospheric carbon in urban areas has become one of the paramount concerns. The planning and management of urban parks and trees to decelerate the worsening impacts of severe carbon emissions have been explored in many different studies [1–7]. For instance, empirical research found that the mean aboveground urban tree carbon stock (dry biomass) across the Seattle urbanizing region was 89 ± 22 Mg C/ha, which is a significant quantity considering the severe atmospheric carbon in city areas [8,9]. Thus, there is now a growing need to study urban green infrastructures and characterize tree species in response to Carbon Storage (CS) variations and their future impacts. Moreover, it is essential to identify the dominant species and their CS potential to ensure environmental equity associated with the resulting ecological benefits [10–12]. Traditionally, information and studies on urban tree structures have used random field sampling and visual interpretation via aerial photos, which are generally expensive, labor intensive, and time-consuming processes and are typically unable to cover a larger area of interest [12–15]. Nevertheless, research on urban tree features, such as their identification, classification, and CS mapping, faces challenges due to the use of non-uniform and multifunctional approaches and a lack of relevant information [12,16].

Recently, Remote Sensing (RS), improved with its latest features (i.e., hyperspectral imagery and high spatial resolution satellite imagery) being introduced as efficient observational and analytical tools, ensuring a robust and easily adaptable means to analyze and identify characteristic vegetation information. Moreover, remote sensing approaches coupled with GIS (Geographic Information Systems) are very useful tools to investigate large areas with reduced time and cost. Tree features, such as their structures (i.e., Height (H), biomass, leaf area, and stems), contributions (i.e., ecological benefits), and arrangements (species abundance and variability) have been identified, classified, and mapped by successfully utilizing remote sensing tools [12,17–22]. Satellite remote sensing has been widely used for tree species identification and classification over the last few decades [23–30]. Even in the case of urban trees, high spatial resolution satellite imagery has been utilized to identify the species along with the individual tree crown extraction [31,32,41,33–40]. However, the classification of urban tree canopy types and species utilizing high spatial resolution satellite imagery faces challenges in urban areas due to their higher urban surface cover heterogeneity, frequent shaded areas of trees and buildings, and the complexity of urban forests compared to natural and planted forests [23,42–46]. Besides, there are also a whole lot of convincing applications of LiDAR-based calibration of the tree CS utilizing the individual tree metrics (i.e.[47–55]). On the other hand, much less evidence is available so far in the case of the calibration of CS of the urban trees

utilizing only the multispectral satellite data; in Iskandar Malaysia, the CS calibration was done based on the WorldView-2 remote sensing data [56]. Despite all these existing methodologies have been already introduced, it is yet a crucial concern to dig out the most convenient and compatible ways to map and predict the urban tree CS in a typical city area. A method could be considered convenient in various ways such as its application, time consumption as well as execution expenses. Even LiDAR application is the most acceptable and widely reliable, it is still expensive and hardly cost-effective for the greater part of the world. That is why, it would be a timely consideration to analyze the utilization of the multispectral satellite data (i.e. Sentinel-2, WorldView-2/3, or Landsat imagery) regarding CS computation possibilities of the trees in an urban area. Here, this doctoral research has been done to introduce an approach to compare different methodologies regarding the estimation of the urban tree biomass as well as the prediction of the possible Carbon Stock (CS) based on the field estimation and mapping utilizing the remote sensing tools in different typical urbanized areas i.e. Sassuolo in Italy as well as in Brussels, Belgium. The main goal of the study is the mapping of the urban tree Carbon Stock (CS) based on field measurements and the application of the Remote Sensing (RS) tools considering the followings:

-A comparative analysis of the application of two different RS tools (i.e. LiDAR & WV3 image data) regarding CS mapping in the same and/or the different urban area;

-Recommending a way out in the case of CS mapping for the policymakers involving urban green management covering a whole city area.

The general idea was to introduce an efficient mapping approach considering the complex urban environment, which will initiate better scopes for the city authority to identify and monitor possible Ecosystem Services (ES) (i.e. CS, canopy-shaded area, etc.) for the dominant tree populations. It is certainly a fact that a tree species map covering a city area with better accuracy is never that much conveniently available. And so urban green planners and researchers must rely on a general urban land cover or vegetation map [57], which leads to a time-consuming and complex approach of mapping any of the ES. For our approach, we have decided to estimate and map CS in urban areas for the existent dominant species considering the tree stand above-ground biomass. At the earlier stage, the mapping methodology was tested in the case of a smaller city area in Sassuolo, Italy. Considering the CS mapping, the high-resolution WV3 image was utilized for classification and identification of the tree species which had been done as a pre-requisite for the species-based CS mapping. Later the estimated CS for the dominant tree species has been completed resulting in a quite authentic map in Sassuolo [58]. However, to find out the efficacy and convenience of the approach in the case of a larger urban area, the CS mapping approach has been utilized in Brussels, Belgium. Insisting on time consumption and cost-effectiveness, a comparative analysis of the mapping outcomes has been illustrated in Brussels where the hyperspectral WV3 image and LiDAR data were available for a similar study area. For the dominant tree species, CS mapping outcomes have been discussed and assessed through a regression analysis among all the Field values and QGIS computations. This mapping approach won't be only an efficient tool in CS mapping but to assist urban planners to ensure the proper utilization of the available green space considering other

valuable prospects of tree species mapping in a complex city environment. Moreover, this study highlights that accurate tree CS mapping is crucial for estimating and identifying the dominant species contributing a significant level of atmospheric CS, which will certainly be a huge support for the urban planners and environmental policymakers in planning further urban air quality assessments. Nevertheless, this doctoral research will contribute to a better understanding of the methodology in mapping structural and functional properties, such as tree CS, as well as predicting the possible urban CS in typical city areas.

Chapter 2.

Literature Review

The world has been experiencing fast-flowing and heedless urbanization for the last few decades. Currently, more than half of the earth's population lives in urban areas, and by 2050, 66 percent will be city dwellers [59]. Overexploitation of environmental resources for the huge population is truly puffing up the vulnerability of the urban dwellers to natural hazards. An efficient and climate-smart urban planning could be the time being and expeditious solution. Conservation and expansion of existing urban and peri-urban vegetation are some of the most effective factors of green urban planning. Green infrastructures, as well as urban vegetations, have a significant impact on the urban climate adaption strategy. Considering climate-smart urban planning strategies, various approaches based on advanced technologies have been implemented to assess the contributions of Urban vegetation especially the trees in the parks and streets. Long-term studies of urban vegetations first began in the U.S. a half-century ago. In the mid-1960s the Street Tree Evaluation Project began evaluating street tree species in five Ohio cities [60]. An assessment of urban forests completed by the City of London showed that the 8 million trees in the urban area produce annual benefits of about £132 million, mostly related to the removal of air pollution, and they have an amenity value estimated at £43 billion [61,62]. Ecosystem Services (ES) provided by the Urban vegetation particularly important in adaptive urban planning, as some benefits crucial for human wellbeing are locally derived, such as rainwater drainage, microclimate regulation, improvement of air quality through pollution removal, noise reduction, and recreation [63]. That is why urban trees and their potential to contribute to human wellbeing in cities are being increasingly acknowledged [64,65]. As the urban trees are solely responsible for the ES of a city, evaluation of their roles in atmospheric CS is one of the prime concerns in respect of climate-smart urban planning. Therefore, it is now a growing need to look for a convenient approach to understand the role of urban trees not only for an efficient urban green management system but also for ensuring the best utilization of the available urban green spaces.

Trees in city streets and parks are now being recognized as a key tool against the egregious impacts of continuous greenspace destruction facing an increased rate of atmospheric carbon concentrations [66–69]. Because they sequester atmospheric carbon during the whole growth process and at the same time delay the adverse effects of climate change contributing to the accumulation of carbon in the soil [2,70,71]. Studies found that the total yearly reduction in carbon emission can be up to 18 kg/tree in urban areas [56,72,73], which clearly brings out the importance of planting trees along with having an efficient tree management policy, especially in a complex city environment.
Through photosynthesis, trees have a direct impact on atmospheric CO_2 fixation, but in urban areas, the process is quite fitful due to tree health issues. As it is well known that the

well-grown trees store far more carbon than the poorly grown ones, it is a huge challenge for the city arborists and policymakers to maintain and preserve mature trees, reforestations, or tree replacements if so as required as well. That is why an efficient and timewise monitoring approach is essential to introduce an adequate urban tree management system [57,74]. And an effective monitoring system could be ensured utilizing an accurate and convenient species-based CS mapping approach. Most of the CS calibration and predictive models are based on the estimation of Above Ground Biomass (AGB) production [73,75–79] which is considered to be mostly responsible for the atmospheric CS [71,80–82]. Currently, Remote Sensing (RS) based intelligent mapping has been implied as an influential approach in monitoring functional and structural urban tree features [83–90]. However, optical RS is unable to estimate the AGB production of trees directly [71,91,92], so many a time studies have been done based on integrating the field estimation with the advanced RS approach [71,93–98]. For instance, in the case of this study, two high-resolution WorldView 3 (WV3) images of two different cities, have been successfully utilized to classify the dominant tree species, which also have been found useful for further CS mapping [58].

In fact, spatially extracted information on tree species over large areas are so significant to understand the roles of the species for example concerning ecosystem functions and services [99–101]. Over the last few decades, RS-based classification of tree species has been widely utilized either in the case of the mapping specific species-based ES outcomes (i.e. [58]), or growth and yield models and, so on (e.g. [99,102,103]). However, in the case of urban areas, tree species mapping is still a huge challenge because of having spatially heterogeneous land cover types from isolated trees to the dense forest; high tree species diversity along with heavily and regularly managed trees as well as the interruptions by buildings and their shadows [69,104–108]. Tree species classification based on spectral properties is quite a matter of contention due to the higher intra-class spectral heterogeneity and/or inter-class spectral similarities [69,106–109]. That is how also the traditional pixel-based procedures, which reckon each class having a distinct spectral signature (ignoring other spatial/contextual information)[110–112], are hardly capable of reaching an acceptable accuracy level [113,114]. Considering these facts, Object-Based Image Analysis (OBIA) approach was introduced in the 1970s, which has been found quite efficient in the case of high-resolution image classifications [110,112,115–118,118]. Instead of the single pixels, the OBIA approach typically works on: (i) segmenting a remote sensing image into spectrally equivalent regions (i.e., segments or objects), and (ii) evaluating the spectral, spatial, and/or context features of these segments for image classification [105,112,113,119,120]. As a result of segmentation, this approach can consider the textual and contextual information along with the spectral information during the classification [112,113,121–123]. That is why OBIA classification results are far better than any of the existing traditional pixel-based approaches [121,124–130]. And so RS approaches especially hyperspectral imagery have significantly beefed up the tree classification outcomes either in the case of single trees or mixed population [99,131–135]. The utilization of very high spatial resolution satellite imagery (e.g., 1-m IKONOS, 0.6-m QuickBird) and aerial photos/digital imagery, have been rapidly increased especially in the case of spatial mapping [109,136–138]. As a matter of fact, recently with the advancements of RS technologies, diversified types of very high resolution remotely sensed images (such

as WorldView-3) are commercially available, certainly introducing a wave of opportunities for the accurate mapping of urban trees at a very significant level [90,99,112,139–142].

Looking up forward especially considering the prospects of an efficient mapping, this doctoral research has been done utilizing the OBIA approach in dominant tree species classification to provide a fundamental tool considering urban CS mapping, which is one of the most important issues for the sustainable urban green management systems and their policymakers.

Chapter 3.

Materials and Methods

3.1. Data set

3.1.1. WV3 image: CS mapping in Sassuolo

The study area was in the city area of Sassuolo, Province of Modena, located in the Po Valley in the northern part of Italy (Figure 1).

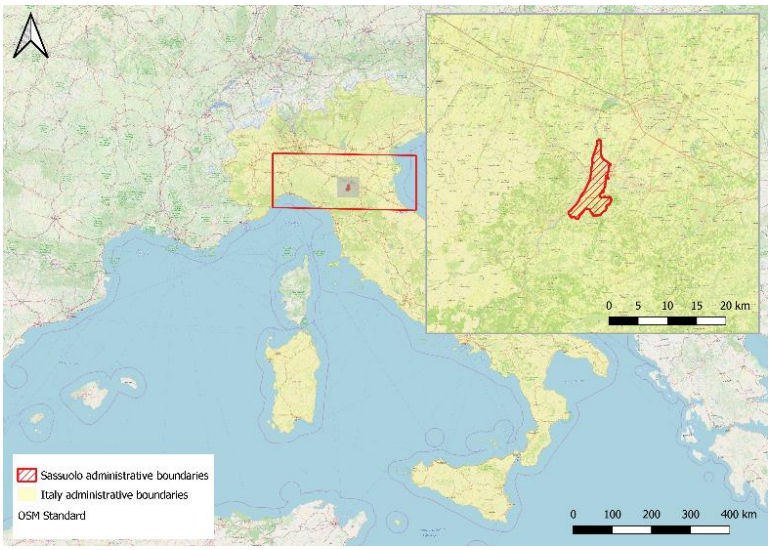

Figure 1. The location of the study area in Sassuolo, Italy [58].

The total investigation area was an urban area of around 273 ha (Figure1). Five dominant tree species (Known as Quercus spp., Acer campestre, Populus nigra, Platanus spp., Tilia platyphyllos) were identified covering all the main streets and the parks.

The key data for this study were the WorldView 3 (WV3) image, shapefiles available from the Geoportal of the Emilia Romagna region [143], and the data collected from the sample plots. Shapefiles were extracted from the CORINE Land Cover (CLC) map [144], a

database of land use of the territory. In this study, artificial surfaces were extracted from the map, such as streets and public green areas. The WV3 image data for this study was acquired on 31 July 2018 (Figure 2). The WV3 includes one panchromatic band of 0.3 m resolution and eight multispectral bands of 1.2 m resolution (Table 1).

Table 1. Eight multispectral bands along with their wavelengths of the WV3 image [58].

Bands	Wavelength(nm)
Coastal band	**400-450**
Blue band	**450-510**
Green band	**510-580**
Yellow band	**585-625**
Red band	**630-690**
Red edge band	**705-715**
Near-Infrared (NIR)1 band	**770-895**
Near-Infrared (NIR)2 band	**860-1040**

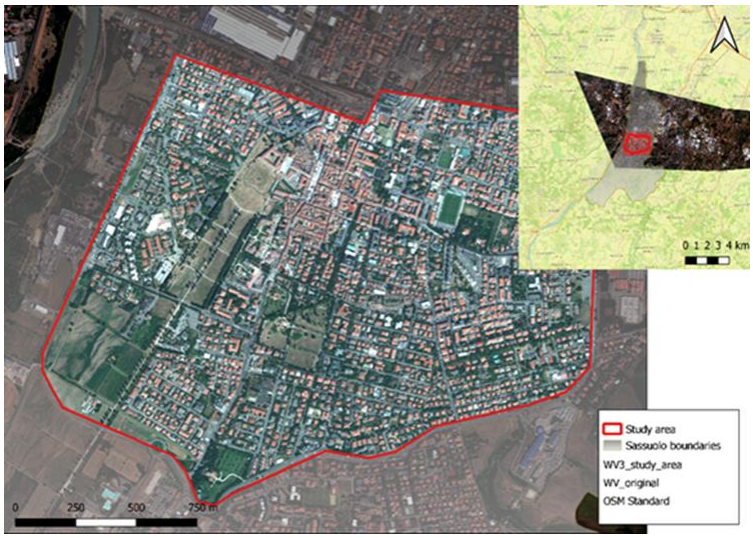

Figure 2. The WV3 image data: the original image and the study area in Sassuolo [58].

For the field data collection, 22 plots of 100m² (10m×10m) each (Figure 3), were randomly selected considering the dominant tree species covering the whole study area of Sassuolo. Among them, 7 plots were considered for the CS mapping and validation. The fundamental considerations were to measure the DBH and H of each tree, along with the geographical coordinates, and to pick out the name of the species. DBH measurements were done at 1.3 m above the ground level. To obtain the H of trees, a photogrammetric approach has been applied. For this purpose, 2D pictures were taken per plot utilizing a hand-held digital camera considering the 3D model development through the Structure-form-Motion (SfM) photogrammetric approach [145]. Several pictures were acquired from different positions, recognizing the shorter to taller trees. The sample plots were also used during the training and validation of the tree species classification.

Figure 3. (a) One of the data sheets showing the plot position (Red square) and trees (Left) along with the required data, (b) sample plots (Red squares) with the validation plots (Yellow squares)[58].

3.1.2. WV3 image: CS mapping in Brussels

The study area, covering an area of around 49 km² in the eastern part of the capital region in Belgium (Figure 4) was selected considering the availability of airborne LiDAR.

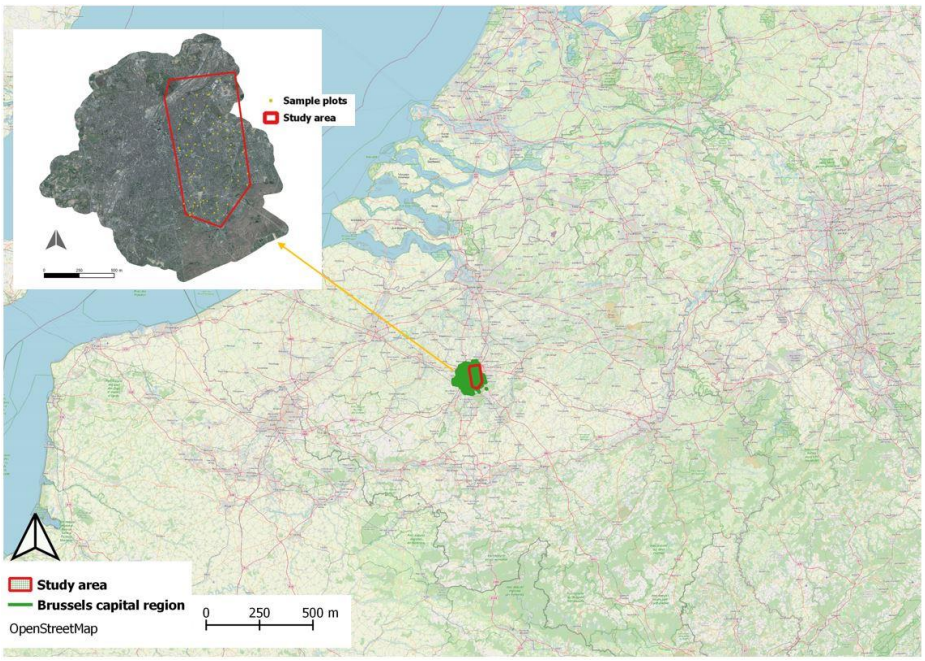

Figure 4. The study area at the eastern part of the urban area showing the locations of the sample plots in Brussels.

The WV3 image data for this study was acquired on 17 April 2017 (Figure 5) which provides one panchromatic band of 0.3 m resolution and eight multispectral bands of 1.2 m resolution as similar as in the case of Sassuolo (Table 1). This time the required shapefiles were educed from the UrbIS database, a general GIS database of the Brussels region [146].

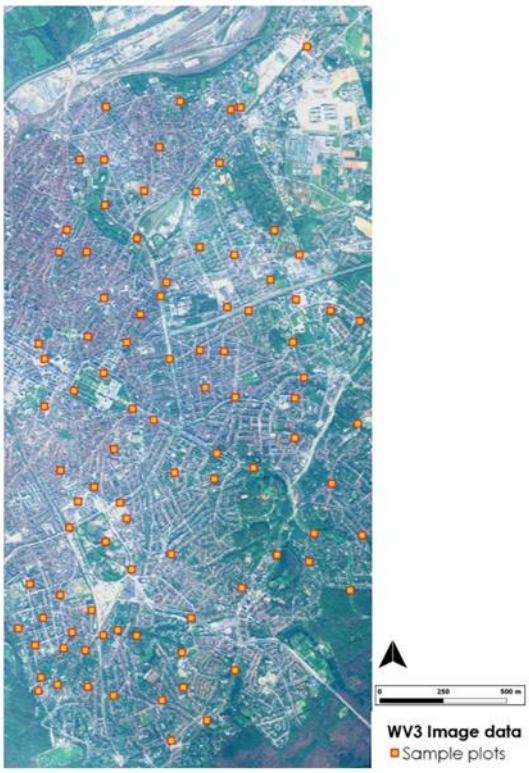

Figure 5. The WV3 image data of the study area in Brussels.

The sample plots were randomly selected covering the streets of the whole study area. Only the street trees were considered because in the parks most of the cases tree crowns were overlapped and or completely overshadowed by the other species. That is why this kind of overcrowded tree population was excluded to avoid the misinterpretations of the species dominance information during the final CS mapping. During the field data collection, 75 plots of 100m² (10m×10m) each (Figure 5), were randomly selected considering the dominant tree species covering the whole study area of Brussels. The sample plots were also used during the training and validation of the tree species classification. Among them, 20 plots were considered for the CS mapping and validation. As earlier, DBH measurements were done at 1.3 m above the ground level. In this case, the H of trees was measured utilizing the 'Nikon Forestry 550' a laser rangefinder with angle compensation technology optimized for forestry use [147] and a field computer was used to mark the plots on QGIS. Field data (H, DBH) were collected in the summer of 2019.

3.1.3. Available LiDAR Data and CS mapping in Brussels

The airborne LiDAR dataset had been collected in Summer 2015 by Aerodata Surveys Nederland BV [148]. The Crown Height Model (CHM; the height of objects) was produced at a resolution of 0.25m using LAStools software [148].

3.2. Methodology

3.2.1. Tree classification and field estimation in Sassuolo

3.2.1(a) Pre-processing

At the earlier stage, the WV3 multispectral image had been processed to convert Digital Numbers into the Top Of Atmosphere (TOA) radiance. Then atmospheric corrections have been performed using the FLAASH plugin of the Environment for Visualizing Images (ENVI) software [149]. In this way, it was possible to retrieve Surface Reflectance (SR). Then some of the required features i.e. The Normalized Difference Vegetation Index (NDVI), the Grey Level Co-occurrence Matrix (GLCM), and the Principal Component Analysis (PCA) for the OBIA classification [25], were computed.

NDVI is a very common vegetation index used in several remote sensing studies [150]. In the case of evaluating a vegetative area, the equation for the calculation of NDVI is as follows:

$$NDVI = \frac{\rho_{NIR} - \rho_{RED}}{\rho_{NIR} + \rho_{RED}}$$

Where,

ρ_{NIR} = reflectance in near-infrared band

ρ_{RED} = reflectance in red band

For this work, several NDVI calculations have been done using both of the (NIR1 and NIR2) Near-Infrared bands along with the red edge band.

GLCM is a tabulation of the frequency of different combinations of grey levels at a specified distance and orientation in an image object [151]. For principal component

analysis, only the first and the second principal components were used. In this way, it was possible to retrieve the less correlated information from the original 8 multispectral bands [152].

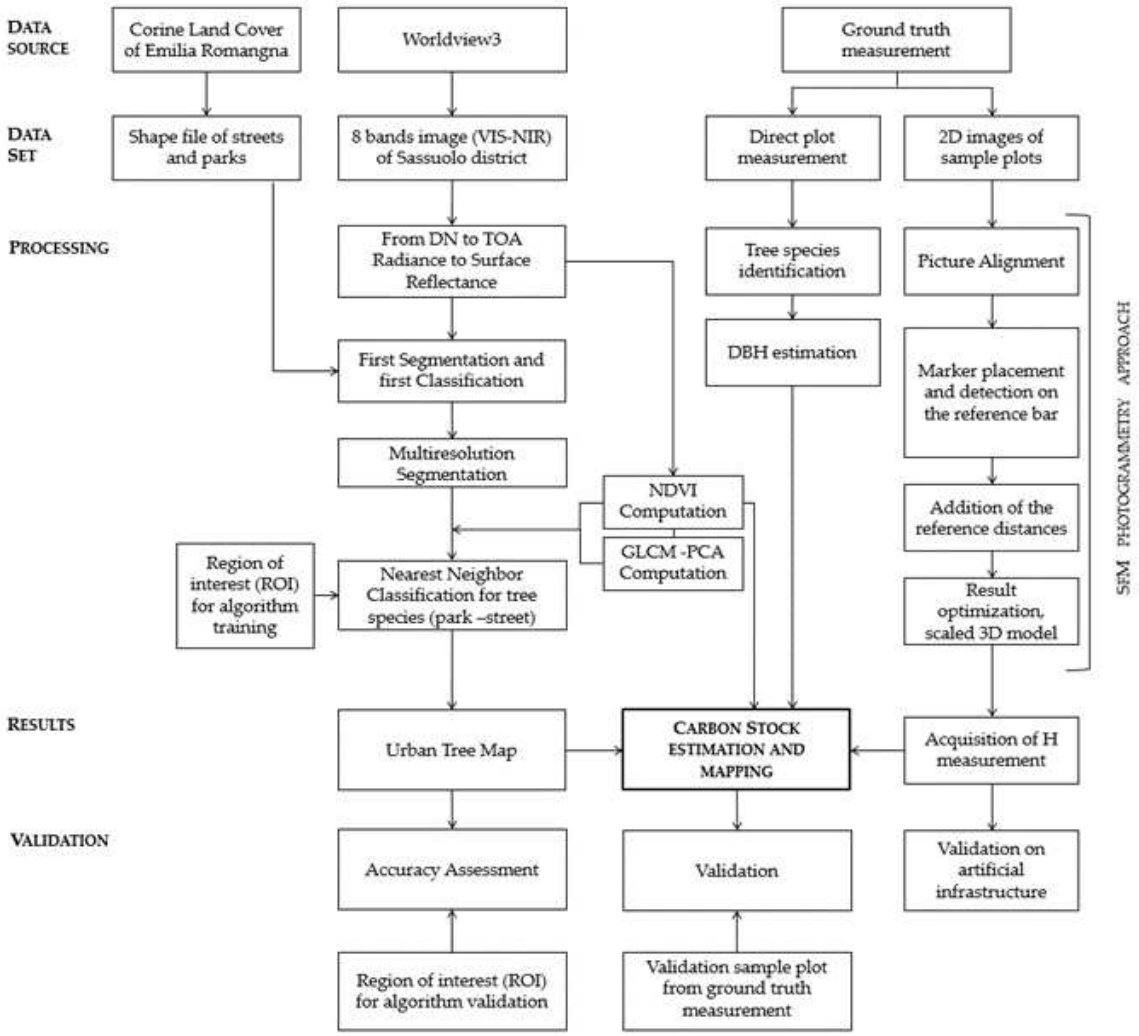

Figure 6. The flowchart of the overall methodology for the Carbon Stock (CS) mapping considering the dominant tree species in Sassuolo[58].

3.2.1(b) Tree species classification in Sassuolo

In urban areas, the traditional pixel-based image classification method usually shows a low classification accuracy due to high spectral variability within the land cover classes[153] which were affected by sun angle, gaps in tree canopies, and shadows [154]. In fact, urban tree classification with higher accuracy is still a considerable challenge, most studies recommend the application of the Object-Based Image Analysis (OBIA) approach to enhance the classification accuracy in urban areas [155–158]. Herein, OBIA approach was also introduced to improve the classification accuracy. The OBIA method includes not only spectral information but also other added information such as context, texture, geometry, and spatial features[35,159], which can minimize the number of units to be considered for the classification[24]. The segmentation is the key procedure to divide the image into different significant objects where the spectral and spatial feature will be computed. The segmentation procedure divides the image into spatially continuous and homogeneous regions [160] and limits the local spectral variation[158,161]. For this study, Trimble eCognition Developer® 9 platform (Trimble, Munich, Germany) [162] was utilized to employ the OBIA approach.

In this study, both the segmentation and classification have been implemented in successive steps to obtain the best results. At first, a chessboard segmentation was carried out using the shapefiles of the Municipality of Sassuolo extracted from the Corine Land Cover (CLC) map of the Emilia-Romagna Region. In particular, the shapefiles of streets and public green areas (i.e. Parks) have been utilized.

Green areas and streets have been identified with very large objects (as the size of the shapefile polygons) and have been classified separately from the rest. In these areas, a subsequent multiresolution segmentation had been applied to have the smaller objects. For this segmentation, instead of the thematic layers, the spectral information and the geometric information of WV3 bands have been considered. After that, considering the study of Li et al [25], the spectral and textural features (NDVIs, GLCM, PCA) have been included to obtain better results in classification. A total of 79 features have been added to the 8 bands of the image.

The result after the second segmentation was smaller objects with a good degree of homogeneity among themselves. Certainly, the resulted medium-sized objects were suitable for the study of tree crowns. The parameters used for segmentation, after numerous tests, were found as scale parameter = 10, shape = 0.2 and the compactness = 0.5.

By using the threshold values for some of the features such as the Brightness and NDVI, the initial classes like shadow, pathways, and grass have been identified. Then, relying on the sample plots, several ground-truth samples (ROIs, Region of Interest) have been chosen for the different tree species. Dominant species have been identified distinctly in the case of parks and roads. It has been done to obtain the classification with better accuracy, as in

parks the tree species diversity is usually higher than those of the streets. In the case of parks, the main classes were identified as-

- *Acer campestre*
- *Populus nigra*
- *Platanus spp.*
- *Quercus spp.*

In the case of streets, the main classes were identified as-

- *Platanus spp.*
- *Quercus spp.*
- *Tilia platyphyllos*

Sample plots had been used for the classification algorithm training where the chosen one was the Nearest Neighbour (NN) algorithm [163].

After the training step, the NN algorithm has been implemented for the assignment of objects to the different classes. The features like the mean and the standard deviation for all bands, the average values of the different NDVI indexes, the Grey Level Co-occurrence Matrix, and the Principal Components were included in the feature space [164]. These features have been chosen to have an improved classification considering the OBIA approach in the case of this study. For instance, the NN algorithm has been used separately for the trees on the parks and streets. It was applied to select the different dominant species for obtaining a more accurate tree species classification. That is why in the classification map, the suffix _street or _park has been used even for the same tree species. In this way, the accuracy of the classification is improved because the sampling points can be chosen separately for parks and streets. Once the classification was done, other samples were used for the validation phase. So, it was possible to calculate the accuracy of the proposed methodology in this area.

3.2.1(c) Photogrammetric approach

For the tree H measurement, SfM photogrammetry approach was introduced in Sassuolo (Figure 6). This approach usually allows the 3D reconstructions of objects through the acquisition of 2D images for the estimation of the required features [145]. In this study, the 3D model was developed for each plot to measure the individual tree H to calibrate the CS utilizing the allometric model [165]. The Agisoft Metashape (AM) software was utilized to produce 3D models implying the SfM algorithm [145,166,167]. In each plot, all the trees

were photographed from different directions, to ensure the maximum data redundancy and the best accuracies. The images were captured with a hand-held, digital SLR camera from photo-points at regular intervals around the perimeter of each plot. A semicircle pathway around each plot successively from the inner to the outer part of the plot was followed to capture each image covering all the trees (Figure 7), images were acquired with different camera inclinations to avoid occlusions. About 120-150 photos/plots were taken depending on the size of the trees.

Figure 7. Dense point clouds of one of the investigated plots (AM model view), the blue squares represent the locations of acquired images [58].

The inner-circle photos were taken from a distance having the tree-top, middle, and bottom part of the tree, and the outer ones to have the whole tree within a frame. This approach ensures a high redundancy of images (each portion of the area of interest must be detected within 9-10 images at least) [145]. Also, a varying viewing geometry must be guaranteed for obtaining accurate results. If no information about camera position or point with known coordinates is added to the project, the reconstructed 3D point cloud will be generated within an arbitrary reference system lacking georeferencing and scale. In this case study, for obtaining a 3D scaled point cloud and measuring the tree H in the 3D model, a 4-meter graduated bar (Figure 8) was added to the area of interest as a reference and depicted in various images. As the positioning of an object of known dimension is an external constraint to the reconstruction allowing the generation of scaled products, the applied methodology is feasible for the measurement purposes of this study [168]. Tree H estimation was done performing the measurements on the reconstructed 3D model.

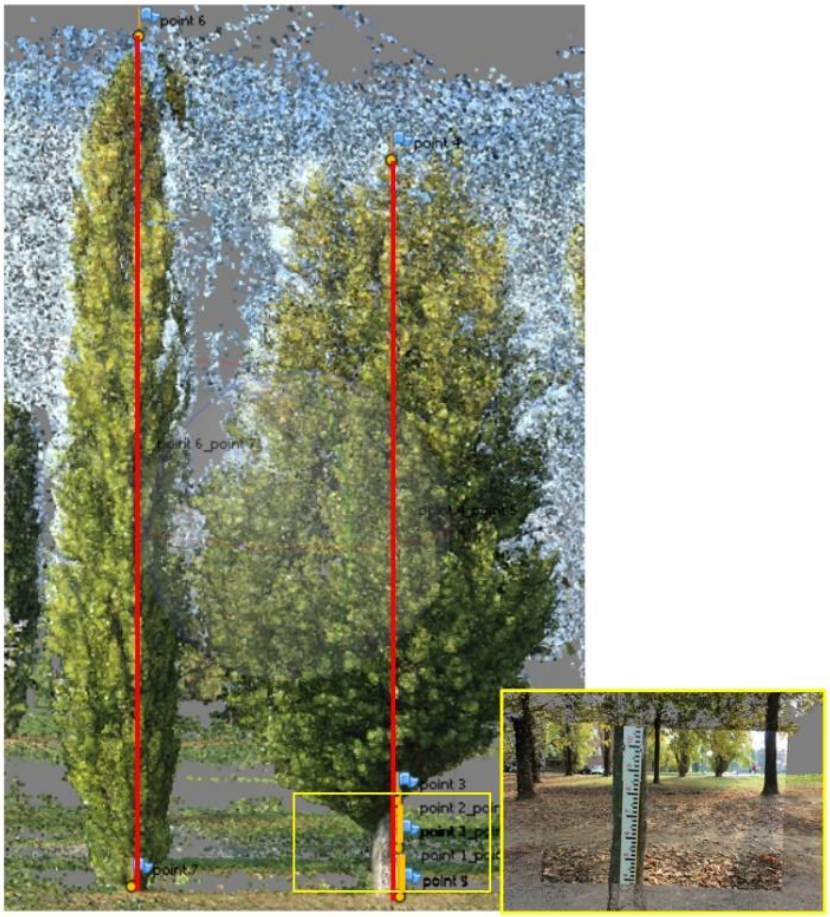

Figure 8. 3D model of the sample plot 4. The blue flags are the added markers and the yellow lines (on the right-side tree's lower trunk) are the segment on the reference bar (Yellow box to show the reference bar) used to constraint the reconstruction and the red lines are the segments created for H estimation [58].

The AM software was used to generate the 3D model for each plot whereas in each model the reference scale bar was visible enough to constraint the reconstruction (Figure 8). From the 3D model, H estimation was done employing the scale creation tool available in AM software. Once the markers were placed on some of the aligned images, the corresponding 3D marker was automatically added to the 3D model. Then, the length of the segment among the points of interest was detected. The identified length was the estimated tree H utilizing the SfM approach.

Validation of the results is mandatory to assess the metric accuracy of the performed measurements. The photogrammetric SfM approach was compared with Laser scanning. A Leica C10 scan station was used for this purpose, the resolution and the accuracy of the resulting point clouds were about a few mm (< 5mm). Laser scanning and Photogrammetry are independent methodologies implying different technologies for the 3D model generation.

Figure 9. Laser scanning 3D point cloud of the test area including the segments (a,b,c,d,e); **Green portion:** the reference scale bar used to constrain the photogrammetric model; **Black lines:** Distances used for the validation purpose [58].

Results obtained with the proposed Photogrammetric methodology were compared with laser scanning technology to validate them and guarantee the metric accuracy of H measurements. The reconstruction of a small portion of a building was performed with both technologies. The validation area was chosen to allow better identification of homologous points. The direct comparison of the generated point clouds does not suit considering this study, so the length of various segments was verified (Figure 9 and Table 2) for a proper investigation of the accuracy of the applied methodology. During the H estimation, the errors were measured considering the estimated values in both cases. Identified differences in the two datasets were about 4 cm, if the longer segments (the ones exceeding 10 m) were taken into consideration, then it would be 6 cm.

Table 2. The results obtained during the metric validation of the obtained 3D models [58].

Segment	Laser scanning	Photogrammetry	Discrepancy
(a)	6.19 m	6.21 m	0.02 m
(b)	13.21 m	13.16 m	0.05 m
(c)	10.38 m	10.45 m	0.07 m
(d)	8.35 m	8.38 m	0.03 m
(e)	5.38 m	5.41 m	0.03 m
	Mean value		**0.04 m**

3.2.2. Tree classification and field estimation in Brussels

3.2.2(a) Pre-processing

In this case, the WV3 image has been pansharpened at the initial stage. Pan-sharpening is the process of merging high-resolution panchromatic and multispectral imagery where the outcome is an image that has the high spectral resolution of the multispectral image and also the high spatial resolution of the panchromatic image [169,170]. The pan sharpen process was conducted using the hyperspectral color sharpening algorithm that combines the high-resolution panchromatic data with lower resolution multispectral data and specifically implemented for WV3 imagery [171]. The cubic convolution resampling technique was chosen to resample the multispectral image to the high-resolution image using a 4x4 pixels moving window. The pan image and the multispectral image have been separately orthorectified using the Digital Surface Model (DSM) downloaded from the GeoPunt portal [172] and from the available LiDAR data. All the steps were conducted in ERDAS Imagine environment [173].

3.2.2 (b) Tree species classification in Brussels

Also, in this case, the Trimble eCognition Developer® 9 platform (Trimble, Munich, Germany) [162] was utilized to classify the dominant tree species in Brussels. As of earlier, the chessboard segmentation has been introduced to initiate the OBIA classification approach. Then the primary classification was done utilizing the available shapefile from the Urbis database [146]. After that, the contrast split segmentation algorithm was implied to define the green and non-green areas with higher accuracy. This is an approach based on the NDVI layer, where the contrast split segments the scene into dark and bright image objects based on a threshold value that maximizes the contrast between them [174]. The algorithm utilizes the optimal threshold separately for each image object which initiates a chessboard segmentation of variable scale and then performs the split on each square

[175,176]. It was found quite useful to identify the shadows, pathways, and pavements in between the tree crowns.

After that, the well-known multiresolution segmentation was performed to group contiguous pixels into areas or segments that are homogenous which is composed of parameters such as the "smoothness/compactness" that determines the preferred shape of segments, and the "color/shape" parameter that controls the weights of spectral and shape information in the calculation of segments' heterogeneity [112,113,177]. After several attempts, the ideal values utilized for segmentation, were found as scale parameter = 10, shape = 0.5 and the compactness = 0.8. Before starting the NN approach, an index known as Canopy Content Chlorophyll Index (CCCI) is used to separate the grasses from the vegetation class. This index can be calibrated as follows,

$$CCCI = \frac{NDRE}{NDVI2}$$

Where,

Normalized Difference Red Edge index [178]

NDRE = NIR2 – Red Edge/ NIR2 + Red Edge,

NDVI2 = NIR2 – Red/ NIR2 + Red

Then the Nearest Neighbour (NN) algorithm [163] was performed which is a supervised classification technique that classified all objects in the entire image based on the selected samples and the defined statistics [113]. For the sample selection and algorithm training, the sample plots had been considered. Once the algorithm training had been done, classification was initiated utilizing the "Assign class" algorithm. Three dominant tree species have been classified as *Tilia spp.*; *Acer spp.* and *Aesculus hippocastanum* covering the whole study area in Brussels. In this case, the larger and in-tensely green parks were not considered as it was hardly possible to differentiate crowns out of a mixed or overlapped tree species population. Also, those trees could not be considered in further CS (AGB estimation) mapping due to the larger difference between the street and the park environment concerning tree health issues.

Validation of the classification outcomes (Table 5) had been done also at the Trimble eCognition Developer® 9 platform [162] using confusion matrices [179–181] which is usually applied to compare the true classes with the ones assigned by the classifier on the generated maps (Detail in section 4.1.2). During the validation,10-15% of the total area for each of the classes had been chosen as "true samples" to train the algorithm. The estimated producer accuracy shows the completeness of classification, and the user accuracy indicates the correctness of the classes [58,182].

3.2.3. CS mapping in urban areas

Several studies suggest that tree AGB is the most visible, dominant, dynamic, and important pool of the terrestrial ecosystem [70,183–185] constituting around 30% of the total terrestrial ecosystem carbon pool [186]. Currently, RS-based biomass assessment has been implied in many studies [71,94,187,188] to obtain forest information over large areas at a reasonable cost with acceptable accuracy and minimal effort [93]. It is also evident that the method of determining relationships between field estimations and RS data-derived variables and then extrapolating these relationships over large areas is very useful [71,95–97,189–193]. In this study, based on the relationships among the WV3 (NDVI) data (In Sassuolo and Brussels) and LiDAR (CHM) data (In Brussels) derived variables and the field data the predictive AGB estimation and eventually, CS mapping have been done in both cases. The comparative analysis between the mapping outcomes of WV3 and LiDAR data has been done in Brussels.

At first, the total Above Ground Biomass (AGB) was calculated based on the field data (i.e., DBH, H, tree species, etc.) for each of the sample plots. For this calculation, an allometric model [165] was implied to calculate the AGB for each plot. The mean AGB/plot estimation was necessary as it is recommended that the tree above ground CS is assumed to be 50% of the total AGB [194–198]. Then to estimate the mean CS/plot, the mean AGB/plot was multiplied by 0.5 as a conversion factor [199–201]. Then in QGIS utilizing the WV3 image data, the NDVI (Red edge and NIR1 band) of the whole study area was computed. The NDVI layer was considered in this study for the CS prediction and mapping, as previous studies claimed to find a strong correlation between the NDVI and total AGB of the trees [56,202–204]. In the case of LiDAR data, the Crown Height Model (CHM) was utilized to map the CS for the dominant tree species.

Then the NDVI-derived metrics were extracted for the sample plots utilizing the 'Zonal statistics' plugin [205] at the QGIS interface. The CHM-derived matrices had been computed in the case of available LiDAR data. After that, the linear regression models were created in Microsoft® Excel™ spreadsheet calibrating the correlation between the mean CS/plot and the NDVI derived metrics to find out the best model to estimate and map the CS covering the whole study area. It has been done also for the CHM-derived matrices to determine the best model concerning the perspective CS mapping. A fishnet of 100m² (10m×10m) resolution (As of the sample plots) was built in QGIS for both cases (NDVI and CHM) to recognize the minimum to the maximum CS zones, based on the dominant species map (Exported as a shapefile in QGIS) obtained from the WV3 image data. The classification shapefile was essential to define the regions of interest which did provide QGIS to map the estimated CS values considering only the dominant tree species. Otherwise, the map will show the CS values for other areas i.e., the area covered with grass or even in the case of an area where there is no vegetation at all.

Later, to validate the mapping outcomes, 20 randomly selected plots have been utilized in both cases (NDVI and CHM). This time the linear regression models were created only for the validation plots. And so, the differences (Table 7 and Table 8) between the QGIS

computed CS values and the ground truth values had been shown to recognize the effectiveness of the methodology. The validation plots were the same in both cases, which was necessary to compare the impacts and to discuss the prospects and convenience of CS mapping in urban areas (Detail in section 4.2.2).

Chapter 4.

Results and Discussion

4.1. Results

4.1.1. SfM approach for tree H estimation in Sassuolo

The results showed that the average H of the was so significant for each of the species (Table 3). The average discrepancies between photogrammetric and Laser Scanning estimated lengths were about some centimeters, which approved the significance of the SfM approach in the case of the tree H estimation[58]. In most cases, marker placement at the treetop was severely responsible for the increased average error. For instance, in the case of the taller trees i.e. *Populus nigra*, the estimated mean H was 29.15m, with an average error of 0.3 to 0.4 cm. In other cases, the average errors were lower except for the overlapping treetops. Unfortunately, there were a few studies on the urban tree H estimation utilizing the SfM approach on AM software, so the general European Forest Tree (EFT) database published in 2016 [206] was considered for this study to have a possible comparison. Even though this database was released based on the forestry areas, comparing the results with the database was not so bland. For instance, for the tree species i.e. *Acer campestre*, *Quercus spp.* and *Populus nigra* the estimated average heights were 10.14, 16.15, and 29.15 meters respectively (Table 3). Whereas according to the EFT database, the average height for the Acer campestre is typically 15 meters and for the Quercus spp. and Populus nigra are 30 and 40 meters respectively [207–209]. Some other recent studies also estimated the average H 18.83 meters for the Quercus spp. and for the Populus nigra the H was mentioned as 23±5 meters in Spain and Sweden respectively [210,211]. The differences among the resulted H of the trees in this study and the H of the other studies are varied possibly due to the following reasons:

• Those studies were done in forestry areas in different environmental conditions;
• In urban areas, the size and shape of the tree crowns got modified in the regular interval;
• In this study, most of the trees were in the streets where frequent tree growth could not be allowed.

Table 3. Estimated (SfM approach) mean H of the dominant species in all the sample plots [58].

Tree species	Mean Height (m)
Quercus spp.	16.15
Acer campestre	10.14
Populus nigra	29.15
Platanus spp.	18.2
Tilia platyphyllos	12.52

4.1.2. OBIA Classification results and validation

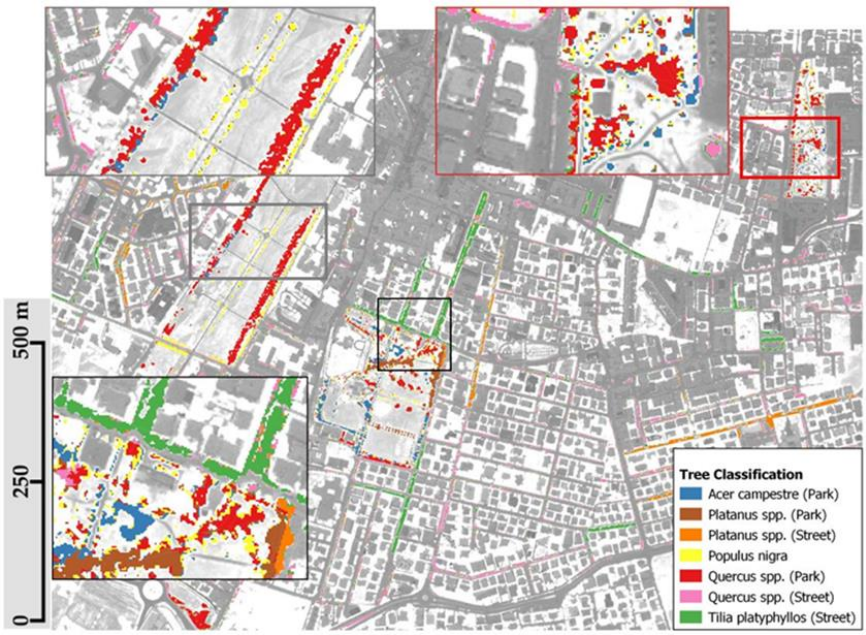

Figure 10. The overall classification obtained with the OBIA approach utilizing the WV3 data for the study area in Sassuolo [58].

In this study, the OBIA approach was implied based on the spectral and textural attributes of the image objects for generating rule sets during the classification. As the WV3 image was from the earlier spring, trees having dead leaves/branches made it quite harder to identify the species in Brussels. And so, species detection was difficult due to the spectral similarities and understory issues. However, the classified map shows that most of the streets are covered with the *Acer spp.* and *Tilia spp.*, while the other species, *Aesculus*

hippocastanum has been mostly observed in the southern part of the city [Figure 11]. While in Sassuolo, species detection was difficult due to the spectral similarities and understory issues. However, 3 dominant tree species in Brussels and 7 dominant tree species have been found with an overall classification accuracy of around 71% and 78% respectively [Figure 10 and Figure 11].

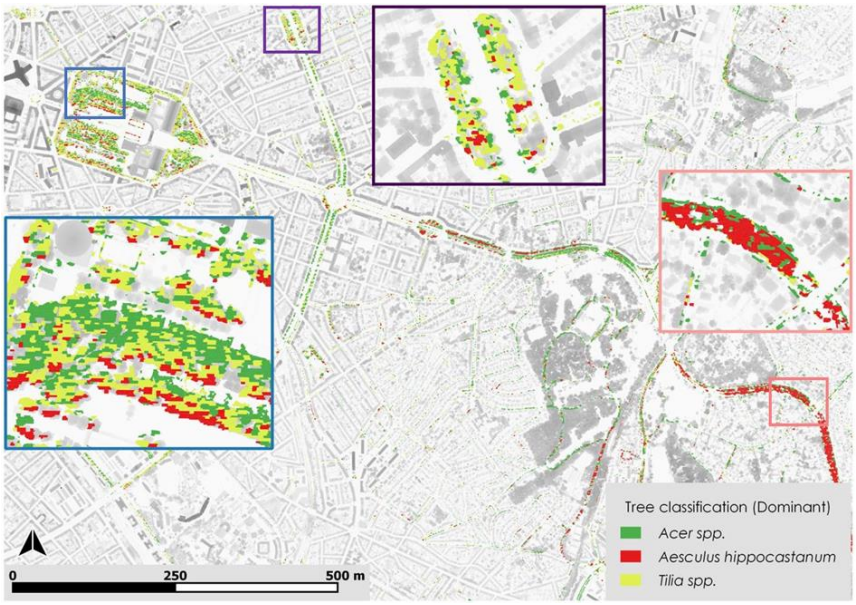

Figure 11. The overall classification obtained with the OBIA approach utilizing the WV3 image data in the case of Brussels.

The classification validation was done through the confusion matrix [179–181] which allows obtaining the overall accuracy of the classification in addition to some parameters of user and producer accuracy. The presence of validation is essential to define the effectiveness of the classification and to know the percentage of error.

Table 4. Validation results expressed in percentage for the trees in Sassuolo [58].

	Populus nigra	***Quercus spp.*** **park**	***Acer campestre*** **park**	***Tilia platyphyllos*** **street**	***Platanus spp.*** **park**	***Quercus spp.*** **street**	***Platanus spp.*** **street**
PA[1]	0.87	0.79	0.68	0.63	0.81	0.70	0.82
UA[1]	0.79	0.89	0.81	0.52	0.73	0.55	0.97
Hellden	0.83	0.83	0.74	0.57	0.77	0.62	0.89
KIA per Class	0.83	0.71	0.65	0.59	0.78	0.68	0.79
Overall Accuracy				**0.78**			
KIA				**0.74**			

[1] PA: Producer Accuracy, UA: User Accuracy.

Validation was carried out only for tree species as representatives of the classes of interest. The areas for validation have been chosen as a percentage equal to 5% of the total area of the tree species through sample plots and deep knowledge of the territory. The validation results are shown in Table 4 for the trees in Sassuolo and Table 5 for the trees in Brussels.

Table 5. Validation results expressed in percentage for the trees in Brussels

	Acer spp.	***Tilia spp.***	***Aesculus hippocastanum***
PA[1]	0.80	0.69	0.67
UA[1]	1	0.69	0.61
Hellden	0.89	0.69	0.64
KIA per Class	0.77	0.42	0.5
Overall Accuracy		**0.71**	
KIA		**0.53**	

[1] PA: Producer Accuracy, UA: User Accuracy.

The producer accuracy indicates the completeness of classification, while the user accuracy indicates the correctness [182]. The Hellden parameter represents the mean accuracy of individual classes. The mean accuracy for class i is calculated by using the equation presented in [212] as,

$$Mean\ accuracy\ (i) = \frac{2A}{B + C} 100\%$$

where A is the number of correctly classified reference points for class i, B is the total number of reference points in class i in the reference data, and C is the total number of reference points classified into class i [213].

KIA is the well-known Kappa Index of Agreement (or Cohen's kappa coefficient) measures the proportion of agreement after chance agreements have been removed from considerations. Kappa increases to one as chance agreement decreases and becomes negative as less than chance agreement occurs [214].

The overall accuracy is the ratio of the sum of diagonal values of the confusion matrix to the total number of cell counts in the matrix. It gives an idea of the accuracy for all the considered classes [215].

4.1.3. Urban CS mapping and validation

4.1.3 (a) CS mapping in Sassuolo

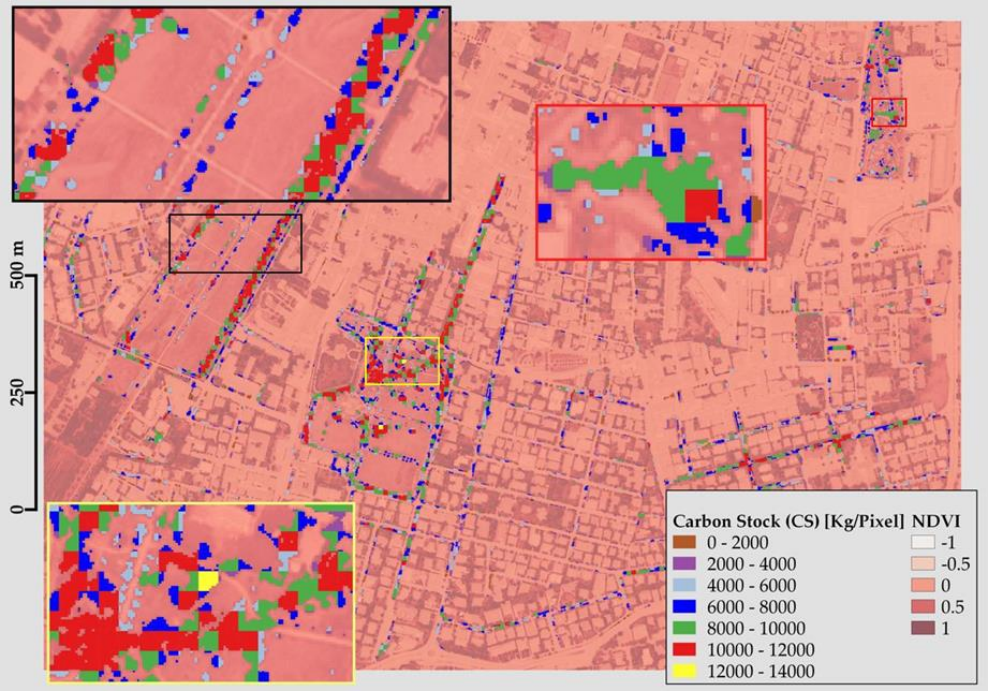

Figure 12. The estimated (QGIS) CS based on different dominant species and their distributions in Sassuolo [58].

CS for the dominant species was calculated and mapped in QGIS showing the intensity of CS based on the species in different zones (Figure 12). Figure 12 shows that the CS map estimated based on the classification shapefile was quite relevant for all the identified dominant species. Especially for those trees which were not shaded or overlapped by the other dominant species, the computed NDVI, as well as the CS mapping, was utterly significant.

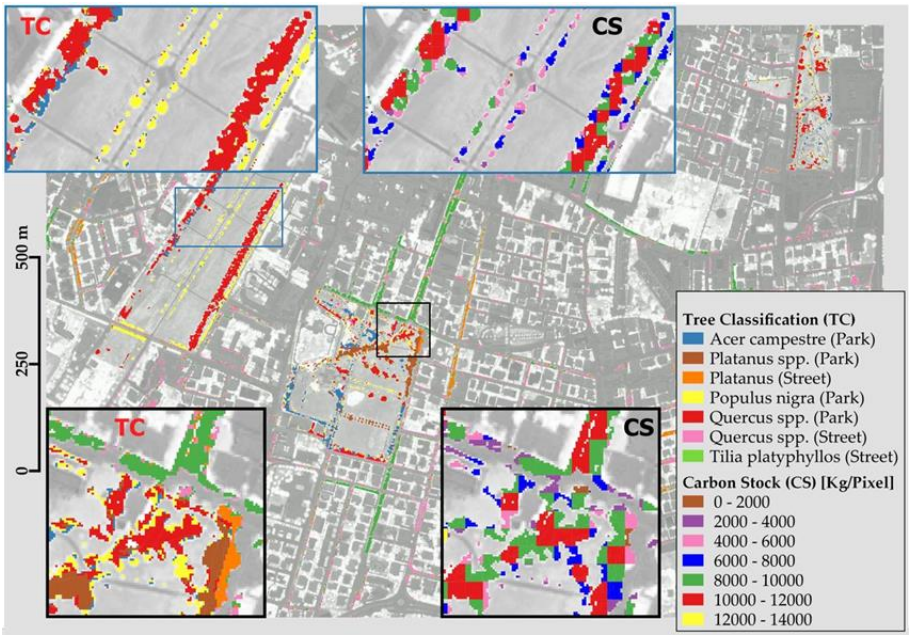

Figure 13. The comparison of estimated CS (QGIS) for the dominant species in the parks and streets of Sassuolo [58].

Among the five dominant species, the species *Quercus spp.*, *Tilia platyphyllos,* and *Platanus spp.* were found to be more responsible for the atmospheric CS covering the areas with higher CS intensity (Red, green, and brown zones at TC in figure 13). Only in the case of *Populus nigra* (Blue and pink zones at CS in figure 13), the values were indicating to moderate to lower CS zones.

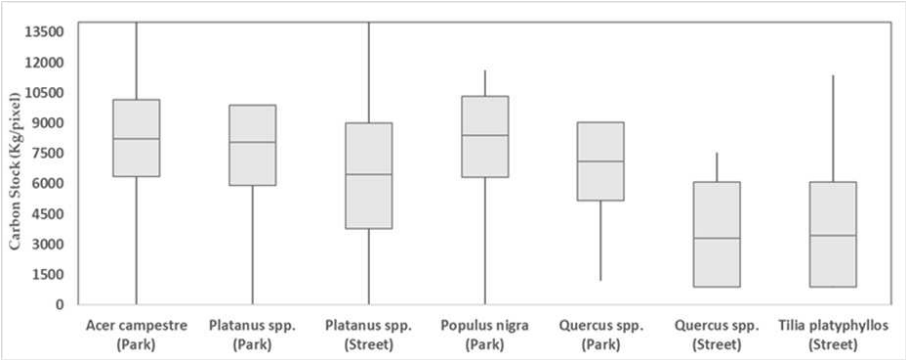

Figure 14. The overall results of the computed CS mapping in QGIS for all the dominant species [58].

The outcome of the CS mapping for the dominant species did approve the reliability of the applied methodology even in the case of a complex urban area (Figure 14). Figure 14 shows the outcome of the CS mapping for the dominant species in the whole urban area represented with a box plot graph. Generally, higher values (see median values for each species) were found for the species i.e. *Acer campestre, Platanus spp., Populus nigra,* and *Quercus spp.* in the parks. Especially, maximum values were found for the *Acer campestre* (park) and the *Platanus spp.* (street), while lower values were found for *Quercus spp.* (street), so as one of the previous studies [216].

For the CS mapping validation, 7 randomly selected plots were considered. Considering all the dominant species, 4 plots from the streets and the other 3 plots were selected from the parks. The results show that the CS estimation in all the cases has a lower difference with the QGIS computed CS values except for plots 5 and 7 which were showing higher differences in the estimations (Table 6). The NDVI based QGIS computation was found to be more applicable in the case of the street trees which are more evident in the WV3 image than the park trees. Smaller species found in parks (i.e. *Acer campestre*) showing higher CS values, which were overlapped by the other dominant species. On the other hand, *Populus nigra*, a taller tree species, showing lower CS values, which was even found as an isolated species with higher CS values during the field estimation.

Table 6. The results obtained during the validation of the estimated CS in the validation plots [58].

Plot id	Tree species	Mean CS/plot (Kg)	CS/plot (Kg) computed in QGIS	Estimation differences (Kg)/plot
1	*Platanus spp.* (Street)	124	180	55
2	*Platanus spp.* (Street)	105	207	102
3	*Platanus spp.* (Street)	655	453	202
4	*Tilia platyphyllos* (Street)	262	361	99
5	*Acer campestre* (Park)	51	375	324
6	*Quercus spp.* (Park)	226	374	148
7	*Populus nigra* (Park)	817	289	528

A regression analysis was done to understand the CS computation efficiency during the mapping. In the case of the street trees, the coefficient of determination was more than 80% (R^2=0.85) where the overall R^2 value was 0.42 considering all the validation plots except the plot with *'Populus nigra'* (Figure 15). The *Populus nigra,* which shows a quite high difference in CS estimation, because of its typical fastigiate structure which is well known as the true 'Lombardy poplar' with a very narrow crown [217]. Having a narrow crown, this species was not so evident which certainly had shown a lower NDVI value leading to a lower computation of CS. But in other cases, the park tree species (i.e. *Acer campestre*) were mixed and adjacent to the other dominant species where the computed NDVI values were significantly higher. Being surrounded by other larger crowns, the small structured species certainly recognizes higher NDVI values. That is why *Acer campestre* also shows a larger difference in the case of the CS estimation which is certainly a shorter tree species than the others. On the other hand, the species on the streets (i.e. *Platanus spp.* and *Tilia platyphyllos*), were found to be isolated and planted having adequate spacing. They were also more evident in the WV3 image showing the lower differences in CS estimation (Table 6). As the validation plots were selected at random, only 2 plots out of the 7 plots had led to the lower R^2 value which clearly true only for those plots. Because in the case of overall CS computation, both species (*Acer campestre* and *Populus nigra*) had been found efficient in the case of atmospheric CS like all the other dominant species (Figure 14). Certainly, the proposed methodology is more efficient (R^2=0.85) in the case of the dominant urban tree species (Figure 14) except for those with overlapped/narrow-crowned (R^2=0.42) structures considering the complex urban environment (Figure 15).

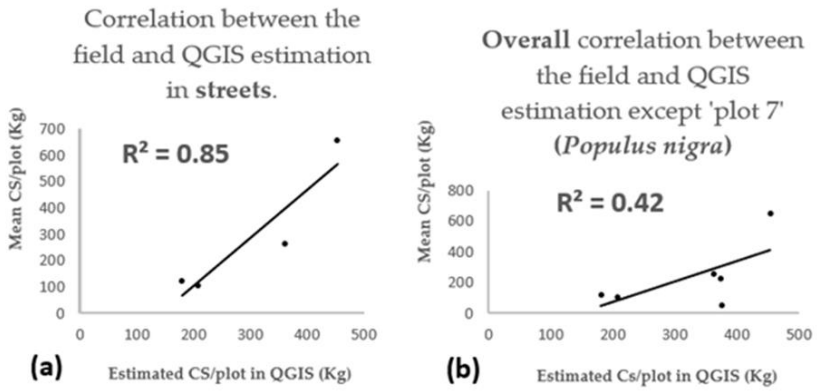

Figure 15: Linear correlation between field estimation and QGIS computation of CS/plot in the case of (a) species in the streets; and among all the trees except 'Populus nigra'(b) in the validation plots [58].

4.1.3 (b) CS mapping in Brussels with WV3 image data

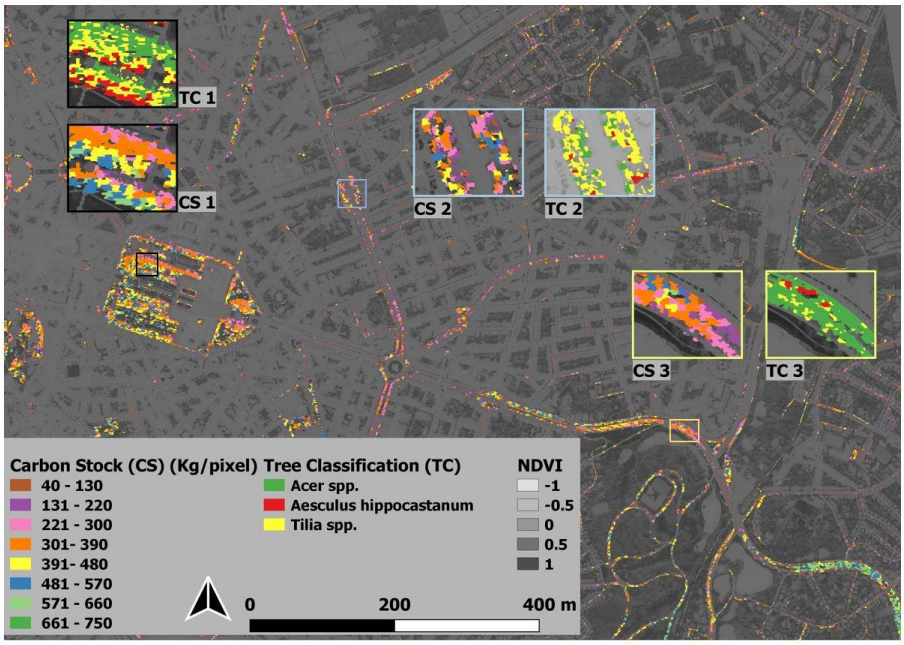

Figure 16. The mapping of the computed CS (QGIS-NDVI) for the dominant species in the streets of Brussels utilizing the WV3 data.

In Brussels, the computed CS for the dominant species has been mapped showing the quantity of CS based on the species in different zones (Figure 16). As far as most of the trees were on the streets, the canopies were not overlapped by the wider crowns. Except for some plots having trees almost leafless or trimmed canopies, the computed CS values based on NDVI derived variables were significant (Figure 16) for most of the dominant species.

In Figure 16, all three-square boxes (As in CS1, CS2, and CS3) are showing moderate (i.e., Pink, Orange, Yellow, and Blue colored zones) to a higher quantity of CS for each of the species (As in TC1, TC2, and TC3). These three zones were zoomed-in considering those plots having comparatively dense canopies, as the WV3 image was ac-quired in early spring, most of the plots were with lighter crowns or leaves.

For the mapping outcome validation, the results (Table 7) show that the field estimation and QGIS computed CS values have apparent variations in few cases. These kinds of differences between the field estimated, and the computed values were quite natural in the case of this study. The field data were collected in the summer of 2019, while the WV3 image was acquired in the earlier spring of 2017. QGIS computation was done based on the NDVI (WV3 data) extracted values where most of the trees were leafless or less green.

Table 7. The results obtained during the validation of the estimated CS in the validation plots.

Plot ID	Tree species	Mean CS (Field estimation) Kg/plot	CS in QGIS estimation (kg/plot)	Difference (Field & QGIS)
1	***Acer spp.***	689.49	426.0	**263.49**
2	***Acer spp.***	930.91	397.8	**533.11**
3	***Acer spp.***	224.04	285.0	**60.96**
4	***Aesculus hippocastanum***	216.95	581.1	**364.15**
5	***Tilia spp.***	302.25	158.2	**144.05**
6	***Acer spp.***	534.17	355.5	**178.67**
7	***Tilia spp.***	277.49	411.9	**134.41**
8	***Acer spp.***	188.18	31.3	**156.88**
9	***Acer spp.***	332.73	242.8	**89.93**
10	***Tilia spp.***	626.63	341.4	**285.23**
11	***Tilia spp.***	277.97	538.8	**260.83**
12	***Tilia spp.***	64.13	214.6	**150.47**
13	***Acer spp.***	698.78	397.8	**300.98**
14	***Aesculus hippocastanum***	641.46	341.4	**300.06**
15	***Tilia spp.***	112.44	271.0	**158.56**
16	***Acer spp.***	466.16	341.4	**124.76**
17	***Tilia spp.***	97.31	45.4	**51.91**
18	***Acer spp.***	121.50	369.6	**248.10**
19	***Aesculus hippocastanum***	577.99	609.3	**31.31**
20	***Acer spp.***	316.80	200.5	**116.30**

As a result, in the case of few plots, NDVI values were quite lower which certainly showed lower CS values during the mapping. Besides, the year gap between the field data (2019)

and the WV3 data (2017) also had a significant impact on the CS mapping outcomes. Because trees in urban areas usually go through the management practices (i.e., Trimming, pruning, etc.) [218], which is also responsible for the larger variations among the field and QGIS computed values (Table 7). For instance, out of the 20 validation plots, only three plots (Plot no. 4, 11, and 18) are showing noticeably more CS/plot than those of the field estimations. Trees in those plots are assumed to be a subject of trimming and or other management practices, which does explain the reasons for having lower AGB or CS/plot in 2019 than those of 2017 for those three plots. A regression analysis had been done to understand the significance of the mapping approach. It was quite noticeable that in most cases where the tree canopies were comparatively evident, even in the early spring season, the percentage of agreement (Figure 17) was more than 80% (R2=0.83). Except for a few cases, this CS mapping approach could be applied in the case of CS mapping even in the case of a complex urban environment.

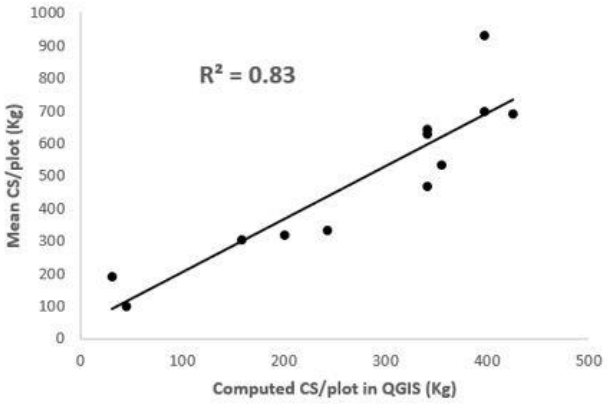

Figure 17: Linear correlation between field estimations and QGIS computations of CS/plot during the validation of CS mapping in Brussels.

4.1.3 (c) CS mapping in Brussels with LiDAR data

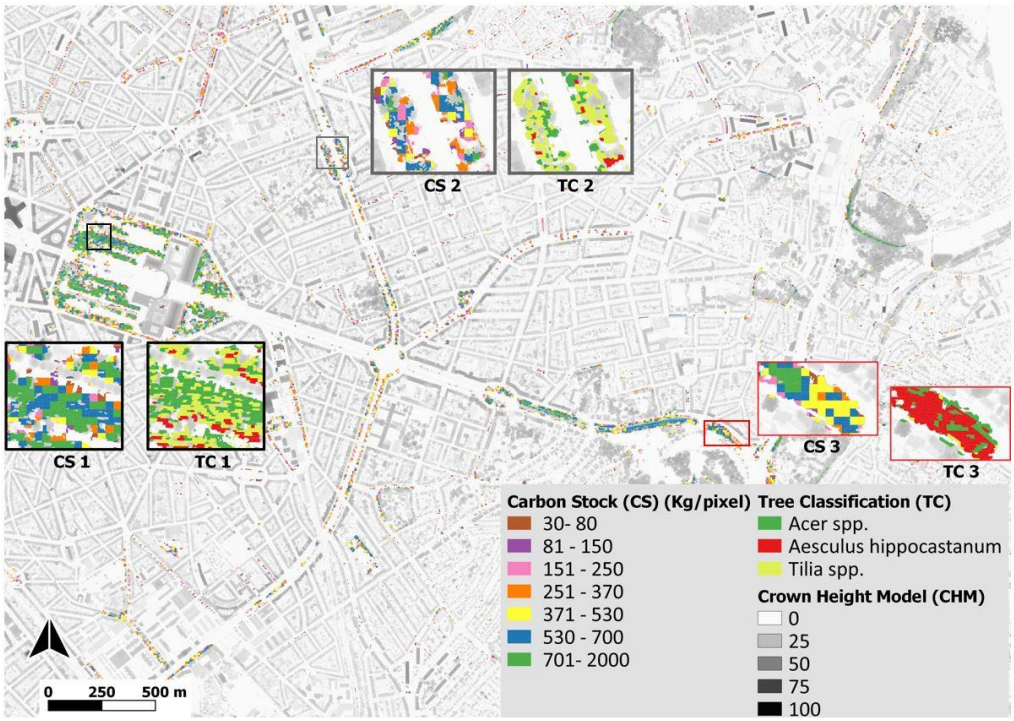

Figure 18. The mapping of the computed CS (QGIS-CHM) for the dominant species in the streets of Brussels utilizing the LiDAR data.

Figure 18 shows that the computed CS map in QGIS was quite relevant also in the case of LiDAR data for all the identified dominant species (TC1, TC2, and TC3 in figure 18). Even the LiDAR data was from 2015, each of the three dominant species had shown evident outcomes in CS mapping (CS1, CS2, and CS3 in figure 18) based on the field data of 2019. As the LiDAR data (From summer 2015) and field data were acquired in summer, the AGB productions per plots were so significant to predict the CS during the mapping based on the CHM- derived variables in QGIS.

For the CS mapping validation, the validation plots were the same ones as earlier in the case of WV3 image data. The outcomes of the validation plots did not show that much difference between the field estimated and QGIS computed values (Table 8). Only a few plots were showing higher differences in the quantity of computed CS which was assumed to be a result of tree crown management practices (i.e., Trimming, pruning, etc.) [218].

Table 8. The results obtained during the estimation of CS in the validation plots.

Plot ID	Tree species	Mean CS (Field estimation) Kg/plot	CS in QGIS estimation (kg/plot)	Difference (Field & QGIS)
1	***Acer spp.***	689.49	761.3	**71.81**
2	***Acer spp.***	930.91	548.6	**382.31**
3	***Acer spp.***	224.04	343.5	**119.46**
4	***Aesculus hippocastanum***	216.95	188.5	**28.45**
5	***Tilia spp.***	302.25	356	**53.75**
6	***Acer spp.***	534.17	675	**140.83**
7	***Tilia spp.***	277.49	283.3	**5.81**
8	***Acer spp.***	188.18	230.9	**42.72**
9	***Acer spp.***	332.73	670.3	**337.57**
10	***Tilia spp.***	626.63	790.2	**163.57**
11	***Tilia spp.***	277.97	462.6	**184.63**
12	***Tilia spp.***	64.13	57.6	**6.53**
13	***Acer spp.***	698.78	696.9	**1.88**
14	***Aesculus hippocastanum***	641.46	179	**462.46**
15	***Tilia spp.***	112.44	200.2	**87.76**
16	***Acer spp.***	466.16	464.5	**1.66**
17	***Tilia spp.***	97.31	188.3	**90.99**
18	***Acer spp.***	121.5	93.9	**27.6**
19	***Aesculus hippocastanum***	577.99	599.4	**21.41**
20	***Acer spp.***	316.8	283.8	**33**

For instance, out of all 20 plots, only 2 plots (Plots no. 2 and 14) were showing noticeable variations between the field and QGIS estimations (Table 8). While in all other plots, trees were showing lower differences in the case of the total atmospheric CS considering the on-plot calibrated values.

A regression analysis was done to understand the relevance of the applied CS mapping approach. It was noticed that the R2 was significantly higher (84 %) excluding 'Plot 2' and 'Plot 14' (Figure 19). In the case of 'Plot 2' and 'Plot 14', the difference between the two estimations is found to be quite higher than those of the others. As earlier, the data acquisition period (2015 and 2019) and the certain tree crown management practices (i.e., Trimming, pruning, etc.) [218] have also been found responsible to have such kind of larger variations. As a result of regular crown trimming practices, the trees even with a wider trunk, in the case of those two plots trees were showing smaller crowns in CHM during the CS computation in QGIS. That is why 'Plot 2', and 'Plot 14' were showing lower CS values than those of the field estimations (Table 8).

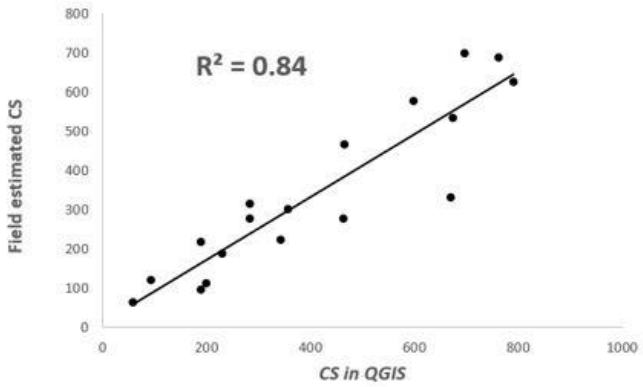

Figure 19: Linear correlation between field estimation and QGIS computation of CS/plot during the validation.

4.2. Discussion

4.2.1. Tree classifications in urban areas

The OBIA approach applied in this study has been applied as an efficient technique in the case of the tree species classification especially for urban areas like Sassuolo [58] and Brussels. The Overall Accuracy (OA) of the thematic mapping was 78% [58] and 71% for both cities respectively (Table 4 and Table 5). For the different classes of species, in Sassuolo the accuracy level varies from higher (89% for the *Platanus spp.*) to the lower (57% for the *Tilia platyphyllos*) and so as in Brussels, the higher one was for the *Acer spp.* (89%) and the lower was for the Aesculus hippocastanum (64%). Usually, the selection of training samples during the NN algorithm has a huge impact on the accuracy of the classification[219]. The quantity of the selected samples must be adequate to allow the algorithm to distinguish among the various classes. Ad hoc samples were chosen for the dominant species in both cases of Brussels and Sassuolo. The spectral characteristics of the different species of trees did show some common traits of spectral response which were too difficult to be differentiated. That is why, the classification features such as NDVI, PCA, and GLCM had been included in the feature space to obtain a classification with better results[25]. Consequently, the OA was more than 70% in both cases which were also significant to go further with the CS mapping.

In the case of the urban areas i.e., in Sassuolo and Brussels like all other European cities, there are numerous species of trees, historic gardens, the vegetation of various types. For instance, in Brussels, the Overall Accuracy (OA) of the species classification was around 71% considering all the identified urban tree species (Table 5). The classification accuracy could be improved (Around 90%) by applying the data fusion (i.e., LiDAR and hyperspectral) approach or estimating OA considering the general urban land cover classification [138–144]. But for this study, the OA was illustrated only for the dominant trees instead of considering the other land cover classes like roads, grasslands, and pavements. Because the main goal of the classification was to identify only the dominant tree species for further CS mapping in QGIS. Unfortunately, studies on urban tree species or genera-based classification (only with multispectral data) with better accuracy (more than 70%) are hardly available, unless the study area is quite smaller (i.e.,[145–147]. Recently, Fang et al [148] have done the tree genera-based classification (From WV3 data) with an OA of 62 to 74% for a larger urban area in Washington D.C., USA. Considering a study area covering almost 49 km², this study in Brussels also could be an acceptable example of approving the efficacy of the OBIA approach. However, the spectral characteristics of the different species did make it quite challenging to distinguish due to their unique phenological ages or conditions [138,150]. In some cases, misinterpretations of desired classes had been identified, which did also recognize the “mixed pixel issues”

where some pixels were not solely covered by one homogeneous class [138,151]. Consequently, with an OA of 71%, this study does show that the WV3 data could be more convenient especially in urban areas, as the WV3 image has an increased level of radiometric, geometric, and spatial (8 bands) resolution leading to classify urban trees at the species level [138,152].

The OBIA approach did distinguish trees from other types of vegetation, yet to differentiate many diversified species could hardly be possible. The common spectral characteristics of many species will make it harder to have a classification with higher accuracy. It is therefore imperative to identify dominant species to reduce errors in classification and to effectively focus on the tree species with higher density in the area.

4.2.2. CS mapping approach: comparative analysis

The methodology implied in this study will have significant impacts on CS calculation[220] and mapping for the dominant species in city areas. The mapping approach in the case of both cities was found to be far convincing than that of the existing traditional approaches. The traditional biomass assessment methods are mostly based on field measurements which are not so convenient or practical to conduct over large areas considering a broad-scale assessment [70,221]. The results in Sassuolo show that the computed CS values were valid and reasonable for almost all the plots except a few cases [58] (Table 6). Considering the dominant species, the CS mapping outcomes were also quite feasible in Brussels where the assessment was highly influenced by the seasonal variations between the data sources (Field and WV3 data). However, in both cases, there were no such factors or issues which could not be sorted out to improve the mapping outcomes. For instance, it is evident that in Brussels, the CS mapping outcomes could have been far valid and significant considering the data sources with similar acquisition periods. In this case, the CS computation utilizing the LiDAR data could be a good example, since there were not that many variations with the field estimations (Table 8). Yet in all cases, there were other noticeable issues like the narrow or too wide and/or small overlapped crowns, trimmed crowns, and so on. These issues are obvious to be considered precisely for any of the urban landscapes [69,106,107] which are heterogeneous in space, structurally, and functionally [109,222–224]. But the proposed RS-based methodology will be implied as more essential and applicable in the case of monitoring and mapping vegetations and their ES than that of the traditional ones.

To date, it is a critical need to develop a high-resolution map of tree biomass within the context of carbon monitoring over terrestrial ecosystems to assess ecosystem response to climate change [225–230], which clearly increases the utilization of the RS-based technologies for the last few decades. For instance, LiDAR data are widely being used to

complete high-resolution surveys of vegetation structure over forested areas and cities [47,231–234], and to estimate biomass and carbon storage in urban vegetation [47,85,235,236] because of its improved accuracy. Even though it is believed that the application of RS is quite expensive in vegetation mapping, Jones et al. (2010) [99,237] found automated methods from combined hyperspectral and LiDAR data (approximately 6 USD per ha) to be competitive against traditional aerial photograph interpretation (approximately 12 USD per ha) in terms of accuracy and cost for a study area in South-western Canada. However, the availability of LiDAR data is not always cost-effective, especially for developing countries. For those cases where LiDAR data is hardly available, high-resolution image data could be a solution for the city policymakers. For instance, studies show that high-resolution commercial data ((Rapid Eye, IKONOS, Geo-eye) are available with an approximate cost of 1–14 € per km2 which is still more affordable than the LiDAR data (62–240 € per km2) [238,239]. So, it could be a better initiative to employ other data sources like WV3 data instead of LiDAR where it is not possible to integrate or to have an available LiDAR da source.

Considering these facts, this doctoral research has been conducted to identify the best outcomes in each case (LiDAR and WV3 image data) and to understand the result discrepancies among the in the similar study area. It is far clear that the mapping outcomes utilizing LiDAR data were much impressive (Table 8) than that of the WV3 data. But still, the regression analysis was showing a significant level of acceptance (Figure 17) also for the WV3 image outcomes in Brussels. Except for only a few plots (3 plots of 20), the percentage of the applicability of the approach was 45% which is certainly not that lower in the case of trees in a complex city environment. On the other hand, the percentage of LiDAR data outcomes except only two plots was more than 80% (Figure 19). But considering the cost-efficiency and the research perspectives, WV3 image data would be more feasible for those developing countries where LiDAR data acquisition is hardly being possible.

Moreover, city planners and managers usually plan to rely on few urban tree attributes i.e. Urban forest structure, green cover, species composition and diversity, available planting spaces, and tree condition to make short- and long-term decisions about the urban forest resource [57]. But at the same time, the costs associated with the data collection and monitoring (Like RS application) have to be compensated by a reduction of field measurement expenses or by an increase in management efficiency that leads to increased income based on improved decision making [99]. That is why the utilization and application of the advanced RS technology depend on the purpose, economic feasibility, and the prospects of the resulted outcomes.

Herein, the proposed methodology will not only show a practical way to understand the contribution of different species in atmospheric CS, but it will also be a way out for the city policymakers especially-

- to introduce and to understand the applicability of a cost-efficient and convenient RS-based approach in the case of urban tree species and their potential CS mapping;
- the estimation of the total benefaction of the individual dominant tree species considering the prediction of the total carbon sequestration;
- understanding the consequences of ensuring adequate plant spacings during the planning of the urban green areas;
- Moreover, identification of the more efficient dominant species considering their roles in urban ecology to utilize the available urban space more noteworthy.

Yet further studies should be done with more sample plots during the field sampling and validation. The CS mapping largely depends on the accuracy of the tree classification, which could be challenging in the case of densely vegetated urban areas. That is why here only the dominant species were taken into consideration. This study was done to understand the perspectives and opportunities of the applied methodology. It would be interesting to find out the CS mapping efficiency in the case of the larger city areas comparing other data sources (i.e. Sentinel, Landsat) with a vast quantity of diversified tree species.

However, the proper understanding of the urban tree species contributions in atmospheric carbon sequestration and storage is one of the most pertinent issues for urban green planning and management[240,241]. This mapping approach could be utilized as a tool to recommend the followings: (Table 9)

- Successful implementation of an RS-based mapping approach especially in urban areas largely depends on the accuracy of the tree species classification and so the quality of the available data sources;
- In the case of an efficient species-based contribution in atmospheric CS, WV3 image data could be a far better and possible solution where the LiDAR data is too inconvenient to employ;
- Especially for the developing countries, to manage and monitor the street and park trees and eventually to estimate the total AGB for the prediction of atmospheric carbon stock (CS), WV3 image data could be a convenient way out for the city authority;
- Moreover, Rs-based (Tree species and their ES) mapping is always the most reliable and comparatively better way either in the case of utilizing the available LiDAR data or a less expensive multiresolution WV3 image data which also influences the sole purpose of mapping.

Table 9: An overview of the doctoral research including the outcomes and recommendations

Approach	Application	Recommendation
-Tree species classification and mapping; -CS estimation and mapping; -Comparative discussion	- Showing the applicability based on cost-efficiency and convenience; - The benefaction of the dominant tree species considering the prediction of the total CS; -AGB estimation and mapping for larger areas	-Dependence of RS approach and mapping on classification accuracy and the quality of the available data sources; -WV3 image data would be more cost-effective and convenient than the LiDAR data; -A way out for the developing countries

A convenient mapping method is a prerequisite not only for the tree CS prediction, but also to understand the roles of the dominant tree species to improve the urban environment considering other ecological benefits. The CS mapping considered in this study could be quite convincing also for the larger city areas, where it is still a big challenge to come up with a map without visiting and marking each tree manually. That is why the mapping effort utilized here will surely introduce an efficient way to initiate proper urban green management and tree plantation systems considering an improved urban atmosphere for the city dwellers.

Chapter 5.

Concluding Remarks

Efficient urban forest and green space management demand adequate data [57,74] where tree inventories are crucial for establishing a strong basis for strategic urban green planning. While CS mapping is time-consuming and tangled with the traditional tree by tree method, this study will ensure a strong baseline to go forward with the tree species classification and CS mapping in urban areas. This study will certainly be recognized considering the prospects of the applied approach based on an efficient (OBIA) classification method for the urban tree species mapping. For instance, the WV3 image with 8 bands (i.e. Coastal band, yellow band, red edge, and NIR2 band) is found to be far suited in the case both of the cities than the traditional four-band ones (usually blue band, green band, red band, and NIR band). Given the estimation of the accuracy level, urban tree species classification outcomes hugely depend on the positions, crown structures, and spectral attributes of the trees. Overlooking those facts, the overall accuracy for the dominant tree species classification for both cities was more than 70%. Also, the CS map reveals that the tree stands levels, species distribution (i.e. in Sassuolo), and temporal variations of the data acquisition period might have a significant influence on the total atmospheric CS for each species in urban areas. Except for a few cases, the proposed methodology would be an adequate solution considering an efficient CS mapping for the dominant urban tree species. This doctoral study was designed to understand and explore the feasibility of the proposed CS mapping approach. It could be an efficient way out for the policymakers in the case of tree species as well as the probable ES mapping in urban areas over the traditional methods. Especially for the developing countries or where the application of LiDAR data is not that cost-effective, this mapping approach will show the alters with WV3 image data. And so, this study outcomes will assist the researchers and city planners to employ and implement the advanced ways of CS mapping for the typical urban areas against the unavoidable impacts of climate change.

References

1. Liu, C.; Li, X. Carbon Storage and Sequestration by Urban Forests in Shenyang, China. *Urban For. Urban Green.* **2012**, *11* (2), 121–128. https://doi.org/10.1016/j.ufug.2011.03.002.
2. Jo, H. K.; Kim, J. Y.; Park, H. M. Carbon Reduction and Planning Strategies for Urban Parks in Seoul. *Urban For. Urban Green.* **2019**, *41*, 48–54. https://doi.org/10.1016/j.ufug.2019.03.009.
3. Nowak, D. J.; Greenfield, E. J.; Hoehn, R. E.; Lapoint, E. Carbon Storage and Sequestration by Trees in Urban and Community Areas of the United States. *Environ. Pollut.* **2013**, *178*, 229–236. https://doi.org/10.1016/j.envpol.2013.03.019.
4. McPherson, E. G.; Simpson, J. R. *Carbon Dioxide Reduction Through Urban Forestry: Guidelines for Professional and Volunteer Tree Planters*; 1999.
5. Gratani, L.; Varone, L.; Bonito, A. Carbon Sequestration of Four Urban Parks in Rome. *Urban For. Urban Green.* **2016**, *19*, 184–193. https://doi.org/10.1016/j.ufug.2016.07.007.
6. Pierdicca, R.; Paolanti, M.; Vaira, R.; Marcheggiani, E.; Malinverni, E. S.; Frontoni, E. Identifying the Use of a Park Based on Clusters of Visitors' Movements from Mobile Phone Data. *J. Spat. Inf. Sci.* **2019**, *2019* (19), 29–52. https://doi.org/10.5311/JOSIS.2019.19.508.
7. Gulinck, H.; Marcheggiani, E.; Verhoeve, A.; Bomans, K.; Dewaelheyns, V.; Lerouge, F.; Galli, A. The Fourth Regime of Open Space. *Sustain.* **2018**, *10* (7). https://doi.org/10.3390/su10072143.
8. Sun, Y.; Xie, S.; Zhao, S. Valuing Urban Green Spaces in Mitigating Climate Change: A City-Wide Estimate of Aboveground Carbon Stored in Urban Green Spaces of China's Capital. *Glob. Chang. Biol.* **2019**, *25* (5), 1717–1732. https://doi.org/10.1111/gcb.14566.
9. Hutyra, L. R.; Yoon, B.; Alberti, M. Terrestrial Carbon Stocks across a Gradient of Urbanization: A Study of the Seattle, WA Region. *Glob. Chang. Biol.* **2011**, *17* (2), 783–797. https://doi.org/10.1111/j.1365-2486.2010.02238.x.
10. Chambers, D.; Périé, C.; Casajus, N.; de Blois, S. Challenges in Modelling the

Abundance of 105 Tree Species in Eastern North America Using Climate, Edaphic, and Topographic Variables. *For. Ecol. Manage.* **2013**, *291*, 20–29. https://doi.org/10.1016/j.foreco.2012.10.046.
11. Van Ewijk, K. Y.; Randin, C. F.; Treitz, P. M.; Scott, N. A. Predicting Fine-Scale Tree Species Abundance Patterns Using Biotic Variables Derived from LiDAR and High Spatial Resolution Imagery. *Remote Sens. Environ.* **2014**, *150*, 120–131. https://doi.org/10.1016/j.rse.2014.04.026.
12. Li, X.; Chen, W. Y.; Sanesi, G.; Lafortezza, R. Remote Sensing in Urban Forestry: Recent Applications and Future Directions. *Remote Sens* **2019**, *11*, 1144.
13. Song, Y.; Imanishi, J.; Sasaki, T.; Ioki, K.; Morimoto, Y. Estimation of Broad-Leaved Canopy Growth in the Urban Forested Area Using Multi-Temporal Airborne LiDAR Datasets. *Urban For* **2016**, *16*, 142–149.
14. Pu, R. L. Mapping Urban Forest Tree Species Using IKONOS Imagery: Preliminary Results. *Environ. Monit. Assess* **2011**, *172*, 199–214.
15. Myeong, S.; Nowak, D. J.; Duggin, M. J. A. Temporal Analysis of Urban Forest Carbon Storage Using Remote Sensing. *Remote Sens* **2006**, *101*, 277–282.
16. Tigges, J.; Lakes, T. High Resolution Remote Sensing for Reducing Uncertainties in Urban Forest Carbon Offset Life Cycle Assessments. *Carbon Balanc. Manag* **2017**, *12*.
17. Singh, K. K.; Chen, G.; McCarter, J. B.; Meentemeyer, R. K. Effects of LiDAR Point Density and Landscape Context on Estimates of Urban Forest Biomass. *ISPRS J. Photogramm* **2015**, *101*, 310–322.
18. Chen, G.; Ozelkan, E.; Singh, K. K.; Zhou, J.; Brown, M. R.; Meentemeyer, R. K. Uncertainties in Mapping Forest Carbon in Urban Ecosystems. *J. Env.* **2017**, *187*, 229–238.
19. Lee, J. H.; Ko, Y. K.; McPherson, E. G. The Feasibility of Remotely Sensed Data to Estimate Urban Tree Dimensions and Biomass. *Urban For* **2016**, *16*, 208–220.
20. Alonzo, M.; McFadden, J. P.; Nowak, D. J.; Roberts, D. A. Mapping Urban Forest Structure and Function Using Hyperspectral Imagery and Lidar Data. *Urban For* **2016**, *17*, 135–147.
21. Solano, F.; Di Fazio, S.; Modica, G. A Methodology Based on GEOBIA and WorldView-3 Imagery to Derive Vegetation Indices at Tree Crown Detail in Olive Orchards. *Int. J. Appl. Earth Obs. Geoinf.* **2019**, *83*, 101912.
22. Modica, G.; Solano, F.; Merlino, A.; Di Fazio, S.; Barreca, F.; Laudari, L.; Fichera, C. R. Using Landsat 8 Imagery in Detecting Cork Oak (Quercus Suber L.) Woodlands: A Case Study in Calabria (Italy). *J. Agric. Eng.* **2016**, *47* (4), 205–215.
23. Pu, R.; Landry, S. A. Comparative Analysis of High Spatial Resolution IKONOS and WorldView-2 Imagery for Mapping Urban Tree Species. *Remote Sens* **2012**, *124*, 516–533.
24. Youjing, Z.; Hengtong, R. Identification Scales for Urban Vegetation Classification Using High Spatial Resolution Satellite Data. *IEEE Int. Geosci. Remote Sens. Symp. 2007*, 1472–1475.
25. Li, D.; Ke, Y.; Gong, H.; Li, X. Object-Based Urban Tree Species Classification Using Bi-Temporal WorldView-2 and WorldView-3 Images. *Remote Sens* **2015**, *7* (12), 16917–16937.
26. Carleer, A.; Wolff, E. Exploitation of Very High-Resolution Satellite Data for Tree

Species Identification. *Photog. Eng* **2004**, *70* (1), 135–140.
27. S0048969717333132.
28. Grace, J. B.; Tilman, D. Perspectives on Plant Competition. *Perspect. plant Compet.* **1990**. https://doi.org/10.2307/4002538.
29. Liang, X.; Jaakkola, A.; Wang, Y.; Hyypp"a, J.; Honkavaara, E.; Liu, J.; Kaartinen, H. The Use of a Hand-Held Camera for Individual Tree 3D Mapping in Forest Sample Plots. *Remote Sens* **2014**, *6*, 6587.
30. Mueed Choudhury, M. A.; Costanzini, S.; Despini, F.; Rossi, P.; Galli, A.; Marcheggiani, E.; Teggi, S. Photogrammetry and Remote Sensing for the Identification and Characterization of Trees in Urban Areas. In *Journal of Physics: Conference Series*; Institute of Physics Publishing, 2019; Vol. 1249. https://doi.org/10.1088/1742-6596/1249/1/012008.
31. Yu, C.; Li, M.; Zhang, M. Classification of Dominant Tree Species in an Urban Forest Park Using the Remote Sensing Image of WorldView-2. In *Proceedings - 2015 8th International Congress on Image and Signal Processing, CISP 2015*; Institute of Electrical and Electronics Engineers Inc., 2016; pp 742–747. https://doi.org/10.1109/CISP.2015.7407976.
32. Katoh, M. Classifying Tree Species in a Northern Mixed Forest Using High-Resolution IKONOS Data. *J.* **2004**, *9*, 7–14.
33. Zhang, C.; Qiu, F. Mapping Individual Tree Species in an Urban Forest Using Airborne LiDAR Data and Hyperspectral Imagery. *Photogramm Eng Remote Sens* **2012**, *78*, 1079–1087.
34. Ikokou, G. B.; Smith, J. A. *Technique for Optimal Selection of Segmentation Scale Parameters for Object-Oriented Classification of Urban Scenes*; Sou. Afri. J. of Geom, 2013.
35. Shojanoori, R.; Shafri, H. Z. M.; Mansor, S.; Ismail, M. H. The Use of WorldView-2 Satellite Data in Urban Tree Species Mapping by Object-Based Image Analysis. *Tech. Sains Malays* **2016**, *45*, 1025–1034.
36. Adeline, K. R. M.; Briottet, X.; Paparoditis, N.; Gastellu-Etchegorry, J. P. Material Reflectance Retrieval in Urban Tree Shadows with Physics-Based Empirical Atmospheric Correction. *IEEE Urban Remote Sens. Event, (JURSE), S{\=a}o Paulo, Brazil, April 2013*, 21–23.
37. Cho, M. A.; Mathieu, R.; Asner, G. P.; Naidoo, L.; Aardt, J. V; Ramoelo, A.; Debba, P.; Wessels, K.; Main, R.; Smit, I. P. J.; et al. Mapping Tree Species Composition in South African Savannas Using an Integrated Airborne Spectral and LiDAR System. *Remote Sens* **2012**, *125*, 214–226.
38. Hao, Z.; Heng-Jia, S.; Bo-Chun, Y. Application of Hyper Spectral Remote Sensing for Urban Forestry Monitoring in Natural Disaster Zones. In *IEEE International Conference on Computer and Management (CAMAN*; 2011; pp 1–4.
39. Kong, C.; Wu, C.; Xu, K. Classification and Extraction of Urban Land-Use Information from High-Resolution Image Based on Multi-Feature of Objects. *Shuju Caiji Yu Chuli/Journal Data Acquis. Process.* **2007**, *22* (3), 315–320.
40. Wania, A.; Weber, C. Hyperspectral Imagery and Urban Green Observation. In *2007 Urban Remote Sensing Joint Event, URS*; 2007. https://doi.org/10.1109/URS.2007.371829.
41. Forzieri, G.; Tanteri, L.; Moser, G.; Catani, F. Mapping Natural and Urban

Environments Using Airborne Multi-Sensor ADS40-MIVIS-LiDAR Synergies. *Int. J. Appl. Earth Obs. Geoinf.* **2013**, *23* (1), 313–323. https://doi.org/10.1016/j.jag.2012.10.004.
42. Du, P.; Xia, J.; Zhang, W.; Tan, K.; Liu, Y.; Liu, S. Multiple Classifier System for Remote Sensing Image Classification: A Review. *Sensors* **2012**, *12*, 4764–4792.
43. Gu, H.; Aditya, S. A.; Townsend, P. A. Detection of Gradients of Forest Composition in an Urban Area Using Imaging Spectroscopy. *Remote Sens* **2015**, *167*, 168–180.
44. Chen, Y.; Wen, D.; Jing, L.; Shi, P. Shadow Information Recovery in Urban Areas from Very High- Resolution Satellite Imagery. *Intern. J. Remote Sens* **2007**, *28* (15), 3249–3254.
45. Adeline, K. R. M.; Chen, M.; Briottet, X.; Pang, S. K.; Paparoditis, N. Shadow Detection in Very High Spatial Resolution Aerial Images: A Comparative Study. ISPRS J. of Photog. and Remote Sens. 2013. *80*, 21–38.
46. Pu, R.; Landry, S.; Yu, Q. *Assessing the Potential of Multi-Seasonal High Resolution Pléiades Satellite Imagery for Mapping Urban Tree Species*; Fifth International Workshop on Earth Observation and Remote Sensing Applications: University of South Florida, Tampa, USA, 2018.
47. Mitchell, M. G. E.; Johansen, K.; Maron, M.; McAlpine, C. A.; Wu, D.; Rhodes, J. R. Identification of Fine Scale and Landscape Scale Drivers of Urban Aboveground Carbon Stocks Using High-Resolution Modeling and Mapping. *Sci. Total Environ.* **2018**, *622*, 57–70.
48. Caynes, R. J. C.; Mitchell, M. G. E.; Wu, D. S.; Johansen, K.; Rhodes, J. R. Using High-Resolution LiDAR Data to Quantify the Three-Dimensional Structure of Vegetation in Urban Green Space. *Urban Ecosyst.* **2016**, *19* (4), 1749–1765. https://doi.org/10.1007/s11252-016-0571-z.
49. Birdal, A. C.; Avdan, U.; Türk, T. Estimating Tree Heights with Images from an Unmanned Aerial Vehicle. *Geomatics, Nat. Hazards Risk* **2017**, *8* (2), 1144–1156.
50. Alonzo, M.; Bookhagen, B.; Roberts, D. A. Urban Tree Species Mapping Using Hyperspectral and Lidar Data Fusion. *Remote Sens. Environ.* **2014**, *148*, 70–83.
51. Kim, S.; McGaughey, R. J.; Andersen, H.-E.; Schreuder, G. Tree Species Differentiation Using Intensity Data Derived from Leaf-on and Leaf-off Airborne Laser Scanner Data. *Remote Sens. Environ.* **2009**, *113* (8), 1575–1586.
52. Plowright, A. A.; Coops, N. C.; Eskelson, B. N. I.; Sheppard, S. R. J.; Aven, N. W. Assessing Urban Tree Condition Using Airborne Light Detection and Ranging. *Urban For. Urban Green.* **2016**, *19*, 140–150.
53. Kim, S.; Hinckley, T.; Briggs, D. Classifying Individual Tree Genera Using Stepwise Cluster Analysis Based on Height and Intensity Metrics Derived from Airborne Laser Scanner Data. *Remote Sens. Environ.* **2011**, *115* (12), 3329–3342.
54. Ørka, H. O.; Næsset, E.; Bollandsås, O. M. Classifying Species of Individual Trees by Intensity and Structure Features Derived from Airborne Laser Scanner Data. *Remote Sens. Environ.* **2009**, *113* (6), 1163–1174.
55. Yao, W.; Krzystek, P.; Heurich, M. Tree Species Classification and Estimation of Stem Volume and DBH Based on Single Tree Extraction by Exploiting Airborne Full-Waveform LiDAR Data. *Remote Sens. Environ.* **2012**, *123*, 368–380.
56. Kanniah, K. D.; Muhamad, N.; CS., K. Remote Sensing Assessment of Carbon

Storage by Urban Forest. *InIOP Conf. Ser. Earth Environ. Sci.* **2014**, *18*, 1.
57. Nitoslawski, S. A.; Galle, N. J.; van den Bosc, C. K.; Steenberg, J. W. N. Smarter Ecosystems for Smarter Cities? A Review of Trends, Technologies, and Turning Points for Smart Urban Forestry. *Sustainable Cities and Society*. Elsevier Ltd November 1, 2019, p 101770. https://doi.org/10.1016/j.scs.2019.101770.
58. Choudhury, M. A. M.; Marcheggiani, E.; Despini, F.; Costanzini, S.; Rossi, P.; Galli, A.; Teggi, S. Urban Tree Species Identification and Carbon Stock Mapping for Urban Green Planning and Management. *Forests* **2020**, *11* (11), 1226. https://doi.org/10.3390/f11111226.
59. 2014 revision of the World Urbanization Prospects | Latest Major Publications - United Nations Department of Economic and Social Affairs https://www.un.org/en/development/desa/publications/2014-revision-world-urbanization-prospects.html.
60. McPherson, E. G.; Berry, A. M.; van Doorn, N. S. Performance Testing to Identify Climate-Ready Trees. *Urban For. Urban Green.* **2018**, *29*, 28–39. https://doi.org/10.1016/j.ufug.2017.09.003.
61. FAO, undefined. Guidelines on Urban and Peri-Urban Forestry. **2016**, undefined-undefined.
62. Rogers, K.; Sacre, K.; Goodenough, J.; Doick, K. Valuing London's Urban Forest: Results of the London i-Tree Eco Project. **2015**.
63. Bolund, P.; Hunhammar, S. *Ecosystem Services in Urban Areas*; 1999; Vol. 29.
64. Tzoulas, K.; Korpela, K.; Venn, S.; Yli-Pelkonen, V.; Kaźmierczak, A.; Niemela, J.; James, P. Promoting Ecosystem and Human Health in Urban Areas Using Green Infrastructure: A Literature Review. *Landscape and Urban Planning*. Elsevier June 20, 2007, pp 167–178. https://doi.org/10.1016/j.landurbplan.2007.02.001.
65. De Vries, S.; van Dillen, S. M. E.; Groenewegen, P. P.; Spreeuwenberg, P. Streetscape Greenery and Health: Stress, Social Cohesion and Physical Activity as Mediators. *Soc. Sci. Med.* **2013**, *94*, 26–33. https://doi.org/10.1016/j.socscimed.2013.06.030.
66. Doick, K. J.; Davies, H. J.; Moss, J.; Coventry, R.; Handley, P.; Vazmonteiro, M.; Rogers, K.; Simpkin, P. *The Canopy Cover of England's Towns and Cities: Baselining and Setting Targets to Improve Human Health and Well-Being*.
67. Endreny, T.; Santagata, R.; Perna, A.; Stefano, C. De; Rallo, R. F.; Ulgiati, S. Implementing and Managing Urban Forests: A Much Needed Conservation Strategy to Increase Ecosystem Services and Urban Wellbeing. *Ecol. Modell.* **2017**, *360*, 328–335. https://doi.org/10.1016/j.ecolmodel.2017.07.016.
68. *Assessing Urban Forest Eff Ects and Values New York City's Urban Forest*.
69. Baines, O.; Wilkes, P.; Disney, M. Quantifying Urban Forest Structure with Open-Access Remote Sensing Data Sets. *Urban For. Urban Green.* **2020**, *50*, 126653. https://doi.org/10.1016/j.ufug.2020.126653.
70. Issa, S.; Dahy, B.; Ksiksi, T.; Saleous, N. A Review of Terrestrial Carbon Assessment Methods Using Geo-Spatial Technologies with Emphasis on Arid Lands. *Remote Sens.* **2020**, *12* (12), 2008. https://doi.org/10.3390/rs12122008.
71. Vicharnakorn, P.; Shrestha, R.; Nagai, M.; Salam, A.; Kiratiprayoon, S. Carbon Stock Assessment Using Remote Sensing and Forest Inventory Data in Savannakhet, Lao PDR. *Remote Sens.* **2014**, *6* (6), 5452–5479.

https://doi.org/10.3390/rs6065452.
72. Rosenfeld, A. H.; Akbari, H.; Romm, J. J.; Pomerantz, M. Cool Communities: Strategies for Heat Island Mitigation and Smog Reduction. *Energy Build.* **1998**, *28* (1), 51–62. https://doi.org/10.1016/S0378-7788(97)00063-7.
73. Francesco Ferrini; Alessio Fini. *Sustainable Management Techniques for Trees in the Urban Areas*.
74. Steenberg, J. W. N.; Duinker, P. N.; Nitoslawski, S. A. Ecosystem-Based Management Revisited: Updating the Concepts for Urban Forests. *Landscape and Urban Planning*. Elsevier B.V. June 1, 2019, pp 24–35. https://doi.org/10.1016/j.landurbplan.2019.02.006.
75. C.L., B.; R.N., J.; J.C., B. DATA COLLECTION AND MANAGEMENT FOR TREE ASSETS IN URBAN ENVIRONMENTS. PROCEEDING URBAN DATA MANAGEMENT SYMPOSIUM January 1, 1999, pp 0–0.
76. Brack, C. L. Pollution Mitigation and Carbon Sequestration by an Urban Forest. *Environ. Pollut.* **2002**, *116* (SUPPL. 1), S195–S200. https://doi.org/10.1016/S0269-7491(01)00251-2.
77. Banks, J. C.; Brack, C. L.; James, R. N. Modelling Changes in Dimensions, Health Status, and Arboricultural Implications for Urban Trees. *Urban Ecosyst.* **1999**, *3* (1), 35–43. https://doi.org/10.1023/A:1009509519236.
78. Nowak, D. J.; Crane, D. E. Carbon Storage and Sequestration by Urban Trees in the USA. In *Environmental Pollution*; Elsevier, 2002; Vol. 116, pp 381–389. https://doi.org/10.1016/S0269-7491(01)00214-7.
79. D.J. Nowak. Chicago's Urban Forest Ecosystem: Results of the Chicago Urban Forest ... - E. Gregory McPherson - Google Books https://books.google.it/books?hl=en&lr=&id=RnT26_xGC-4C&oi=fnd&pg=PA83&ots=G9uEFurr1T&sig=4B7P3Onwpe9Qp84zgMYDsorMViw&redir_esc=y#v=onepage&q&f=false (accessed Jan 9, 2021).
80. Mokany, K.; Raison, R. J.; Prokushkin, A. S. Critical Analysis of Root: Shoot Ratios in Terrestrial Biomes. *Glob. Chang. Biol.* **2006**, *12* (1), 84–96. https://doi.org/10.1111/j.1365-2486.2005.001043.x.
81. Achard, F.; Eva, H. D.; Stibig, H. J.; Mayaux, P.; Gallego, J.; Richards, T.; Malingreau, J. P. Determination of Deforestation Rates of the World's Humid Tropical Forests. *Science (80-.).* **2002**, *297* (5583), 999–1002. https://doi.org/10.1126/science.1070656.
82. Brown, S. *Estimating Biomass and Biomass Change of Tropical Forests: A Primer*; Food & Agriculture Org., 1997; Vol. 134.
83. Liu, L.; Coops, N. C.; Aven, N. W.; Pang, Y. Mapping Urban Tree Species Using Integrated Airborne Hyperspectral and LiDAR Remote Sensing Data. *Remote Sens. Environ.* **2017**, *200*, 170–182. https://doi.org/10.1016/j.rse.2017.08.010.
84. Alonzo, M.; Bookhagen, B.; Roberts, D. A. Urban Tree Species Mapping Using Hyperspectral and Lidar Data Fusion. *Remote Sens. Environ.* **2014**, *148*, 70–83. https://doi.org/10.1016/j.rse.2014.03.018.
85. Alonzo, M.; McFadden, J. P.; Nowak, D. J.; Roberts, D. A. Mapping Urban Forest Structure and Function Using Hyperspectral Imagery and Lidar Data. *Urban For. Urban Green.* **2016**, *17*, 135–147. https://doi.org/10.1016/j.ufug.2016.04.003.
86. Zhang, Y.; Shen, W.; Li, M.; Lv, Y. Assessing Spatio-Temporal Changes in Forest

Cover and Fragmentation under Urban Expansion in Nanjing, Eastern China, from Long-Term Landsat Observations (1987–2017). *Appl. Geogr.* **2020**, *117*, 102190. https://doi.org/10.1016/j.apgeog.2020.102190.
87. Zhang, M.; Du, H.; Mao, F.; Zhou, G.; Li, X.; Dong, L.; Zheng, J.; Zhu, D.; Liu, H.; Huang, Z.; et al. Spatiotemporal Evolution of Urban Expansion Using Landsat Time Series Data and Assessment of Its Influences on Forests. *ISPRS Int. J. Geo-Information* **2020**, *9* (2), 64. https://doi.org/10.3390/ijgi9020064.
88. Shen, G.; Wang, Z.; Liu, C.; Han, Y. Mapping Aboveground Biomass and Carbon in Shanghai's Urban Forest Using Landsat ETM+ and Inventory Data. *Urban For. Urban Green.* **2020**, *51*, 126655. https://doi.org/10.1016/j.ufug.2020.126655.
89. Ren, Z.; Zheng, H.; He, X.; Zhang, D.; Yu, X.; Shen, G. Spatial Estimation of Urban Forest Structures with Landsat TM Data and Field Measurements. *Urban For. Urban Green.* **2015**, *14* (2), 336–344. https://doi.org/10.1016/j.ufug.2015.03.008.
90. He, S.; Du, H.; Zhou, G.; Li, X.; Mao, F.; Zhu, D.; Xu, Y.; Zhang, M.; Huang, Z.; Liu, H.; et al. Intelligent Mapping of Urban Forests from High-Resolution Remotely Sensed Imagery Using Object-Based U-Net-DenseNet-Coupled Network. *Remote Sens.* **2020**, *12* (23), 3928. https://doi.org/10.3390/rs12233928.
91. *Towards Participatory Forest Management in Laos-Laos Country Report 2003-: 44~54 Institute for Global Environmental Strategies*; 2004.
92. Ramankutty, N.; Gibbs, H. K.; Achard, F.; Defries, R.; Foley, J. A.; Houghton, R. A. Challenges to Estimating Carbon Emissions from Tropical Deforestation. *Global Change Biology*. John Wiley & Sons, Ltd January 1, 2007, pp 51–66. https://doi.org/10.1111/j.1365-2486.2006.01272.x.
93. Lu, D. The Potential and Challenge of Remote Sensing-Based Biomass Estimation. *International Journal of Remote Sensing*. Taylor and Francis Ltd. April 10, 2006, pp 1297–1328. https://doi.org/10.1080/01431160500486732.
94. Wannasiri, W.; Nagai, M.; Honda, K.; Santitamnont, P.; Miphokasap, P. Extraction of Mangrove Biophysical Parameters Using Airborne LiDAR. *Remote Sens.* **2013**, *5* (4), 1787–1808. https://doi.org/10.3390/rs5041787.
95. Foody, G. M.; Boyd, D. S.; Cutler, M. E. J. Predictive Relations of Tropical Forest Biomass from Landsat TM Data and Their Transferability between Regions. *Remote Sens. Environ.* **2003**, *85* (4), 463–474. https://doi.org/10.1016/S0034-4257(03)00039-7.
96. Kobayashi, S.; Omura, Y.; Sanga-Ngoie, K.; Widyorini, R.; Kawai, S.; Supriadi, B.; Yamaguchi, Y. Characteristics of Decomposition Powers of L-Band Multi-Polarimetric SAR in Assessing Tree Growth of Industrial Plantation Forests in the Tropics. *Remote Sens.* **2012**, *4* (10), 3058–3077. https://doi.org/10.3390/rs4103058.
97. Clewley, D.; Lucas, R.; Accad, A.; Armston, J.; Bowen, M.; Dwyer, J.; Pollock, S.; Bunting, P.; McAlpine, C.; Eyre, T.; et al. An Approach to Mapping Forest Growth Stages in Queensland, Australia through Integration of ALOS PALSAR and Landsat Sensor Data. *Remote Sens.* **2012**, *4* (8), 2236–2255. https://doi.org/10.3390/rs4082236.
98. Das, S.; Singh, T. P. Correlation Analysis between Biomass and Spectral Vegetation Indices of Forest Ecosystem. *Int. J. Eng. Res. Technol.* **2012**, *1* (5).
99. Fassnacht, F. E.; Latifi, H.; Stereńczak, K.; Modzelewska, A.; Lefsky, M.; Waser,

L. T.; Straub, C.; Ghosh, A. Review of Studies on Tree Species Classification from Remotely Sensed Data. *Remote Sensing of Environment*. Elsevier Inc. December 1, 2016, pp 64–87. https://doi.org/10.1016/j.rse.2016.08.013.

100. Van Ewijk, K. Y.; Randin, C. F.; Treitz, P. M.; Scott, N. A. Predicting Fine-Scale Tree Species Abundance Patterns Using Biotic Variables Derived from LiDAR and High Spatial Resolution Imagery. *Remote Sens. Environ.* **2014**, *150*, 120–131. https://doi.org/10.1016/j.rse.2014.04.026.
101. Chambers, D.; Périé, C.; Casajus, N.; de Blois, S. Challenges in Modelling the Abundance of 105 Tree Species in Eastern North America Using Climate, Edaphic, and Topographic Variables. *For. Ecol. Manage.* **2013**, *291*, 20–29. https://doi.org/10.1016/j.foreco.2012.10.046.
102. Vauhkonen, J.; Ørka, H. O.; Holmgren, J.; Dalponte, M.; Heinzel, J.; Koch, B. Tree Species Recognition Based on Airborne Laser Scanning and Complementary Data Sources; Springer, Dordrecht, 2014; pp 135–156. https://doi.org/10.1007/978-94-017-8663-8_7.
103. Ørka, H. O.; Dalponte, M.; Gobakken, T.; Næsset, E.; Ene, L. T. Characterizing Forest Species Composition Using Multiple Remote Sensing Data Sources and Inventory Approaches. *Scand. J. For. Res.* **2013**, *28* (7), 677–688. https://doi.org/10.1080/02827581.2013.793386.
104. Myeong, S.; Nowak, D.; Hopkins, P.; Brock, R. Urban Cover Mapping Using Digital, High-Spatial Resolution Aerial Imagery. *Urban Ecosyst.* **2001**, *5* (4), 243–256. https://doi.org/10.1023/A:1025687711588.
105. Qian, Y.; Zhou, W.; Nytch, C. J.; Han, L.; Li, Z. A New Index to Differentiate Tree and Grass Based on High Resolution Image and Object-Based Methods. *Urban For. Urban Green.* **2020**, *53*, 126661. https://doi.org/10.1016/j.ufug.2020.126661.
106. Shafri, H. *Review on the Use of Remote Sensing for Urban Forest Monitoring Urban Sprawl Assessment View Project Modeling of CO Emissions from Traffic Vehicles Using Artificial Neural Networks View Project*.
107. Wilkes, P.; Disney, M.; Vicari, M. B.; Calders, K.; Burt, A. Estimating Urban above Ground Biomass with Multi-Scale LiDAR. *Carbon Balance Manag.* **2018**, *13* (1), 10. https://doi.org/10.1186/s13021-018-0098-0.
108. Zhu, Z.; Zhou, Y.; Seto, K. C.; Stokes, E. C.; Deng, C.; Pickett, S. T. A.; Taubenböck, H. Understanding an Urbanizing Planet: Strategic Directions for Remote Sensing. *Remote Sens. Environ.* **2019**, *228*, 164–182. https://doi.org/10.1016/j.rse.2019.04.020.
109. Qian, Y.; Zhou, W.; Pickett, S. T. A.; Yu, W.; Xiong, D.; Wang, W.; Jing, C. Integrating Structure and Function: Mapping the Hierarchical Spatial Heterogeneity of Urban Landscapes. *Ecol. Process.* **2020**, *9* (1), 1–11. https://doi.org/10.1186/s13717-020-00266-1.
110. Jebur, M. N.; Mohd Shafri, H. Z.; Pradhan, B.; Tehrany, M. S. Per-Pixel and Object-Oriented Classification Methods for Mapping Urban Land Cover Extraction Using SPOT 5 Imagery. *Geocarto Int.* **2014**, *29* (7), 792–806. https://doi.org/10.1080/10106049.2013.848944.
111. Wang, L.; Sousa, W. P.; Gong, P. Integration of Object-Based and Pixel-Based Classification for Mapping Mangroves with IKONOS Imagery. *Int. J. Remote Sens.* **2004**, *25* (24), 5655–5668. https://doi.org/10.1080/01431160233129121 5.

112. Johnson, B.; Jozdani, S. Identifying Generalizable Image Segmentation Parameters for Urban Land Cover Mapping through Meta-Analysis and Regression Tree Modeling. *Remote Sens.* **2018**, *10* (2), 73. https://doi.org/10.3390/rs10010073.
113. Makinde, E. O.; Salami, A. T.; Olaleye, J. B.; Okewusi, O. C. Object Based and Pixel Based Classification Using Rapideye Satellite Imager of ETI-OSA, Lagos, Nigeria. *Geoinformatics FCE CTU* **2016**, *15* (2), 59–70. https://doi.org/10.14311/gi.15.2.5.
114. Blaschke, T.; Lang, S.; Lorup, E.; Strobl, J.; Zeil, P. Object-Oriented Image Processing in an Integrated GIS/Remote Sensing Environment and Perspectives for Environmental Applications. **2000**.
115. Estoque, R. C.; Murayama, Y.; Akiyama, C. M. Pixel-Based and Object-Based Classifications Using High- and Medium-Spatial-Resolution Imageries in the Urban and Suburban Landscapes. *Geocarto Int.* **2015**, *30* (10), 1113–1129. https://doi.org/10.1080/10106049.2015.1027291.
116. Li, X.; Meng, Q.; Gu, X.; Jancso, T.; Yu, T.; Wang, K.; Mavromatis, S. A Hybrid Method Combining Pixel-Based and Object-Oriented Methods and Its Application in Hungary Using Chinese HJ-1 Satellite Images. *Int. J. Remote Sens.* **2013**, *34* (13), 4655–4668. https://doi.org/10.1080/01431161.2013.780669.
117. Jabari, S.; Zhang, Y. Very High Resolution Satellite Image Classification Using Fuzzy Rule-Based Systems. *Algorithms* **2013**, *6* (4), 762–781. https://doi.org/10.3390/a6040762.
118. Platt, R. V.; Rapoza, L. An Evaluation of an Object-Oriented Paradigm for Land Use/Land Cover Classification. *Prof. Geogr.* **2008**, *60* (1), 87–100. https://doi.org/10.1080/00330120701724152.
119. Wieland, M.; Pittore, M. Performance Evaluation of Machine Learning Algorithms for Urban Pattern Recognition from Multi-Spectral Satellite Images. *Remote Sens.* **2014**, *6* (4), 2912–2939. https://doi.org/10.3390/rs6042912.
120. Gao, Y.; Mas, J. F. *A COMPARISON OF THE PERFORMANCE OF PIXEL-BASED AND OBJECT-BASED CLASSIFICATIONS OVER IMAGES WITH VARIOUS SPATIAL RESOLUTIONS*.
121. Han, R.; Liu, P.; Wang, G.; Zhang, H.; Wu, X. Advantage of Combining OBIA and Classifier Ensemble Method for Very High-Resolution Satellite Imagery Classification. *J. Sensors* **2020**, *2020*, 1–15. https://doi.org/10.1155/2020/8855509.
122. Hossain, M. D.; Chen, D. Segmentation for Object-Based Image Analysis (OBIA): A Review of Algorithms and Challenges from Remote Sensing Perspective. *ISPRS Journal of Photogrammetry and Remote Sensing*. Elsevier B.V. April 1, 2019, pp 115–134. https://doi.org/10.1016/j.isprsjprs.2019.02.009.
123. Kucharczyk, M.; Hay, G. J.; Ghaffarian, S.; Hugenholtz, C. H. Geographic Object-Based Image Analysis: A Primer and Future Directions. *Remote Sens.* **2020**, *12* (12), 2012. https://doi.org/10.3390/rs12122012.
124. Blaschke, T. Object Based Image Analysis for Remote Sensing. *ISPRS Journal of Photogrammetry and Remote Sensing*. Elsevier January 1, 2010, pp 2–16. https://doi.org/10.1016/j.isprsjprs.2009.06.004.
125. Fu, B.; Wang, Y.; Campbell, A.; Li, Y.; Zhang, B.; Yin, S.; Xing, Z.; Jin, X. Comparison of Object-Based and Pixel-Based Random Forest Algorithm for Wetland Vegetation Mapping Using High Spatial Resolution GF-1 and SAR Data.

Ecol. Indic. **2017**, *73*, 105–117. https://doi.org/10.1016/j.ecolind.2016.09.029.
126. Duro, D. C.; Franklin, S. E.; Dubé, M. G. A Comparison of Pixel-Based and Object-Based Image Analysis with Selected Machine Learning Algorithms for the Classification of Agricultural Landscapes Using SPOT-5 HRG Imagery. *Remote Sens. Environ.* **2012**, *118*, 259–272. https://doi.org/10.1016/j.rse.2011.11.020.
127. Myint, S. W.; Gober, P.; Brazel, A.; Grossman-Clarke, S.; Weng, Q. Per-Pixel vs. Object-Based Classification of Urban Land Cover Extraction Using High Spatial Resolution Imagery. *Remote Sens. Environ.* **2011**, *115* (5), 1145–1161. https://doi.org/10.1016/j.rse.2010.12.017.
128. Martins, V. S.; Kaleita, A. L.; Gelder, B. K.; da Silveira, H. L. F.; Abe, C. A. Exploring Multiscale Object-Based Convolutional Neural Network (Multi-OCNN) for Remote Sensing Image Classification at High Spatial Resolution. *ISPRS J. Photogramm. Remote Sens.* **2020**, *168*, 56–73. https://doi.org/10.1016/j.isprsjprs.2020.08.004.
129. Su, T.; Liu, T.; Zhang, S.; Qu, Z.; Li, R. Machine Learning-Assisted Region Merging for Remote Sensing Image Segmentation. *ISPRS J. Photogramm. Remote Sens.* **2020**, *168*, 89–123. https://doi.org/10.1016/j.isprsjprs.2020.07.017.
130. de Pinho, C. M. D.; Fonseca, L. M. G.; Korting, T. S.; de Almeida, C. M.; Kux, H. J. H. Land-Cover Classification of an Intra-Urban Environment Using High-Resolution Images and Object-Based Image Analysis. *Int. J. Remote Sens.* **2012**, *33* (19), 5973–5995. https://doi.org/10.1080/01431161.2012.675451.
131. Adelabu, S.; Mutanga, O.; Adam, E.; Cho, M. A. Exploiting Machine Learning Algorithms for Tree Species Classification in a Semiarid Woodland Using RapidEye Image. *J. Appl. Remote Sens.* **2013**, *7* (1), 073480. https://doi.org/10.1117/1.jrs.7.073480.
132. Carleer, A.; Wolff, E. Exploitation of Very High Resolution Satellite Data for Tree Species Identification. *Photogramm. Eng. Remote Sensing* **2004**, *70* (1), 135–140. https://doi.org/10.14358/PERS.70.1.135.
133. Ghosh, A.; Fassnacht, F. E.; Joshi, P. K.; Kochb, B. A Framework for Mapping Tree Species Combining Hyperspectral and LiDAR Data: Role of Selected Classifiers and Sensor across Three Spatial Scales. *Int. J. Appl. Earth Obs. Geoinf.* **2014**, *26* (1), 49–63. https://doi.org/10.1016/j.jag.2013.05.017.
134. Jensen, R. R.; Hardin, P. J.; Hardin, A. J. Classification of Urban Tree Species Using Hyperspectral Imagery. *Geocarto Int.* **2012**, *27* (5), 443–458. https://doi.org/10.1080/10106049.2011.638989.
135. Somers, B.; Asner, G. P. Tree Species Mapping in Tropical Forests Using Multi-Temporal Imaging Spectroscopy: Wavelength Adaptive Spectral Mixture Analysis. *Int. J. Appl. Earth Obs. Geoinf.* **2014**, *31* (1), 57–66. https://doi.org/10.1016/j.jag.2014.02.006.
136. Zhou, W.; Troy, A. An Object-Oriented Approach for Analysing and Characterizing Urban Landscape at the Parcel Level. *Int. J. Remote Sens.* **2008**, *29* (11), 3119–3135. https://doi.org/10.1080/01431160701469065.
137. Ouma, Y. O.; Tateishi, R. Urban-Trees Extraction from Quickbird Imagery Using Multiscale Spectex-Filtering and Non-Parametric Classification. *ISPRS J. Photogramm. Remote Sens.* **2008**, *63* (3), 333–351. https://doi.org/10.1016/j.isprsjprs.2007.10.006.

138. Lee, D. S.; Shan, J.; Bethel, J. S. Class-Guided Building Extraction from Ikonos Imagery. In *Photogrammetric Engineering and Remote Sensing*; American Society for Photogrammetry and Remote Sensing, 2003; Vol. 69, pp 143–150. https://doi.org/10.14358/PERS.69.2.143.
139. Degerickx, J.; Hermy, M.; Somers, B. Mapping Functional Urban Green Types Using High Resolution Remote Sensing Data. *Sustainability* **2020**, *12* (5), 2144. https://doi.org/10.3390/su12052144.
140. Puissant, A.; Rougiera, S.; Stumpf, A. Object-Oriented Mapping of Urban Trees Using Random Forestclassifiers. *Int. J. Appl. Earth Obs. Geoinf.* **2014**, *26* (1), 235–245. https://doi.org/10.1016/j.jag.2013.07.002.
141. Pu, R.; Landry, S. Mapping Urban Tree Species by Integrating Multi-Seasonal High Resolution Pléiades Satellite Imagery with Airborne LiDAR Data. *Urban For. Urban Green.* **2020**, *53*, 126675. https://doi.org/10.1016/j.ufug.2020.126675.
142. Pu, R.; Landry, S. A Comparative Analysis of High Spatial Resolution IKONOS and WorldView-2 Imagery for Mapping Urban Tree Species. *Remote Sens. Environ.* **2012**, *124*, 516–533. https://doi.org/10.1016/j.rse.2012.06.011.
143. Home — GeoER https://geoportale.regione.emilia-romagna.it/it (accessed Mar 3, 2020).
144. Bossard, M.; Feranec, J.; Corine, O. J. *Land Cover Technical Guide---Addendum 2000;* 2000.
145. Choudhury, M. A. M.; Costanzini, S.; Despini, F.; Rossi, P.; Galli, A.; Marcheggiani, E.; Teggi, S. P.; Sensing, R. For the Identification and Characterization of Trees in Urban Areas. *J. Phys* **2019**, *1249*.
146. UrbIS Download http://urbisdownload.gis.irisnet.be/en/temporality/ (accessed Nov 16, 2020).
147. Nikon | News | Nikon Introduces New Laser Rangefinder “Forestry 550” https://www.nikon.com/news/2008/0924_forestry_02.htm (accessed Nov 16, 2020).
148. Degerickx, J.; Roberts, D. A.; McFadden, J. P.; Hermy, M.; Somers, B. Urban Tree Health Assessment Using Airborne Hyperspectral and LiDAR Imagery. *Int. J. Appl. earth Obs. Geoinf.* **2018**, *73*, 26–38.
149. Inc, R. S. *No Title*; RSI)ENVI user guide, 2003.
150. Brivio, P.; LECHI-LECHI, G.; Zilioli, E. *Principi e Metodi Di Telerilevamento*; CittaStudi, 2006.
151. Ke, Y.; Quackenbush, L. J.; Im, J. Synergistic Use of QuickBird Multispectral Imagery and LIDAR Data for Object-Based Forest Species Classification. *Remote Sens. Environ.* **2010**, *114* (6), 1141–1154.
152. Eeti, L. N.; Buddhiraju, K. M.; Bhattacharya, A. A Single Classifier Using Principal Components Vs Multi-Classifier System: In Landuse-LandCover Classification of WorldView-2 Sensor Data. *ISPRS Ann. Photogramm. Remote Sens. Spat. Inf. Sci.* **2014**, *2* (8), 91.
153. Yu, Q.; Gong, P.; Clinton, N.; Biging, G.; Kelly, M.; Schirokauer, D. Object-Based Detailed Vegetation Classification with Airborne High Spatial Resolution Remote Sensing Imagery. Photogram. *Engin. Rem* **2006**, *72*, 799–811.
154. Johnson, B.; Xie, Z. Classifying a High-Resolution Image of an Urban Area Using Super-Object Information. *ISPRS J. Photogram. Rem* **2013**, *83*, 40–49.
155. segmentation, L. A. I. And Discriminant Analysis for the Identification of Land

Cover Units in Ecology. *IEEE Trans Geosci. Remote Sens* **1997**, *35*, 1136–1145.
156. Puissant, A.; Rougier, S.; Stumpf, A. Object-Oriented Mapping of Urban Trees Using Random Forest Classifiers. *Intern. Jour. Appl. Earth Obs. Geoinform* **2014**, *26*, 235–245.
157. Shouse, M.; Liang, L.; Fei, S. Identification of Understory Invasive Exotic Plants with Remote Sensing in Urban Forests. *Intern. J. Appl. Earth Obs. Geoinform* **2013**, *21*, 525–534.
158. Li, C.; Yin, J.; Zhao, J. Extraction of Urban Vegetation from High Resolution Remote Sensing Image. In *International Conference on Computer Design and Applications (ICCDA) 4*; 2010; pp 403–406.
159. Zhou, W. An Object-Based Approach for Urban Land Cover Classification: Integrating LiDAR Height and Intensity Data. IEEE Geosc. and Rem. *Sens* **2013**, *10* (4), 928–931.
160. Flanders, D.; Hall-Beyer, M.; Perverzoff, J. Preliminary Evaluation of ECognition Object- Based Software for Cut Block Delineation and Feature Extraction. *Cana. Jour. Rem* **2003**, *29* (4), 441–452.
161. Lobo, A. I. segmentation. And Discriminant Analysis for the Identification of Land Cover Units in Ecology. *IEEE Trans Geosci. Remote Sens* **1997**, *35*, 1136–1145.
162. AG., D. *ECognition Version 5 Object Oriented Image Analysis User Guide. 2005*; Munich: Germany.
163. Blanzieri, E.; Melgani, F. Nearest Neighbor Classification of Remote Sensing Images with the Maximal Margin Principle. *IEEE Trans. Geosci. Remote Sens.* **2008**, *46* (6), 1804–1811.
164. Peterson, E. B. M. Structure-from-Motion Photogrammetry for Three-Dimensional Structure of Lichens and Change over Time. *Bryologist* **2019**, *122* (2), 325–339.
165. Tabacchi, G.; Cosmo, D.; Gasparini, L. .; tree volume, P. A. And Phytomass Prediction Equations for Forest Species in Italy. *Eur. J. For. Res* **2011**, *130*, 911–934.
166. Miller, J.; Morgenroth, J.; Gomez, C. 3d. Modelling of Individual Trees Using a Handheld Camera: Accuracy of Height, Diameter and Volume Estimates. *Urban Fores* **2015**, *14*, 932–940.
167. Westoby, M. J.; Brasington, J.; Glasser, N. F.; Hambrey, M. J.; Reynolds, J. M. Structure-from-Motion. *Photogramm. A low-cost, Eff. tool Geosci. Appl.* **2012**, *179*, 300–314.
168. Castagnetti, C.; Rossi, P.; Capra, A. 3d. Reconstruction of Rock Paintings: A Cost-Effective Approach Based on Modern Photogrammetry for Rapidly Mapping Archaeological Findings. *IOP Conf. Ser. Mater. Sci. Eng. (Vol.* **2018**, *364*, 1.
169. Gilbertson, J. K.; Kemp, J.; van Niekerk, A. Effect of Pan-Sharpening Multi-Temporal Landsat 8 Imagery for Crop Type Differentiation Using Different Classification Techniques. *Comput. Electron. Agric.* **2017**, *134*, 151–159. https://doi.org/10.1016/j.compag.2016.12.006.
170. Karakus, P.; Karabork, H. EFFECT OF PANSHARPENED IMAGE ON SOME OF PIXEL BASED AND OBJECT BASED CLASSIFICATION ACCURACY. *ISPRS - Int. Arch. Photogramm. Remote Sens. Spat. Inf. Sci.* **2016**, *XLI-B7*, 235–239. https://doi.org/10.5194/isprs-archives-xli-b7-235-2016.
171. Padwick, C.; Deskevich, M.; Pacifici, F.; Smallwood, S. WorldView-2 Pan-

Sharpening. In *Proceedings of the ASPRS 2010 Annual Conference, San Diego, CA, USA*; 2010; Vol. 2630, pp 1–14.
172. Geopunt.be – The Flemish Geoportal | con terra https://www.con-terra.com/casestudies/geopuntbe-flemish-geoportal (accessed Jan 9, 2021).
173. ERDAS IMAGINE: World-Class Remote Sensing Software | Hexagon Geospatial https://www.hexagongeospatial.com/products/power-portfolio/erdas-imagine/erdas-imagine-remote-sensing-software-package (accessed Jan 9, 2021).
174. Basic Rule Set Editing https://docs.ecognition.com/v9.5.0/eCognition_documentation/User Guide Developer/4 Basic Rule Set Editing.htm (accessed Nov 17, 2020).
175. El-naggar, A. M. Determination of Optimum Segmentation Parameter Values for Extracting Building from Remote Sensing Images. *Alexandria Engineering Journal*. Elsevier B.V. December 1, 2018, pp 3089–3097. https://doi.org/10.1016/j.aej.2018.10.001.
176. Huang, J.; Zhang, X.; Xin, Q.; Sun, Y.; Zhang, P. Automatic Building Extraction from High-Resolution Aerial Images and LiDAR Data Using Gated Residual Refinement Network. *ISPRS J. Photogramm. Remote Sens.* **2019**, *151*, 91–105. https://doi.org/10.1016/j.isprsjprs.2019.02.019.
177. Benz, U. C.; Hofmann, P.; Willhauck, G.; Lingenfelder, I.; Heynen, M. Multi-Resolution, Object-Oriented Fuzzy Analysis of Remote Sensing Data for GIS-Ready Information. *ISPRS J. Photogramm. Remote Sens.* **2004**, *58* (3–4), 239–258. https://doi.org/10.1016/j.isprsjprs.2003.10.002.
178. Carneiro, F. M.; Furlani, C. E. A.; Zerbato, C.; de Menezes, P. C.; Gírio, L. A. d. S. Correlations among Vegetation Indices and Peanut Traits during Different Crop Development Stages. *Eng. Agric.* **2019**, *39* (specialissue), 33–40. https://doi.org/10.1590/1809-4430-ENG.AGRIC.V39NEP33-40/2019.
179. Gupta, D. L.; Malviya, A. K.; Singh, S. Performance Analysis of Classification Tree Learning Algorithms. *Int. J. Comput. Appl.* **2012**, *1*, 55.
180. Immitzer, M.; Vuolo, F.; Atzberger, C. First Experience with Sentinel-2 Data for Crop and Tree Species Classifications in Central Europe. *Remote SensingMar;* **2016**, *8*, 3.
181. So-In, C.; Mongkonchai, N.; Aimtongkham, P.; Wijitsopon, K.; Rujirakul, K. An Evaluation of Data Mining Classification Models for Network Intrusion Detection. In *In2014 fourth international conference on digital information and communication technology and its applications (DICTAP)May 6*; Ieee. [Google Scholar, 2014; pp 90–94.
182. Foody, G. Assessing the Accuracy of Remotely Sensed Data: Principles and Practices. *Photogramm. Rec.* **2010**, *25* (130), 204–205. https://doi.org/10.1111/j.1477-9730.2010.00574_2.x.
183. Kumar, L.; Mutanga, O. Remote Sensing of Above-Ground Biomass. *Remote Sens.* **2017**, *9* (9), 935. https://doi.org/10.3390/rs9090935.
184. Cairns, M. A.; Brown, S.; Helmer, E. H.; Baumgardner, G. A. Root Biomass Allocation in the World's Upland Forests. *Oecologia* **1997**, *111* (1), 1–11. https://doi.org/10.1007/s004420050201.
185. Fonton, N. H.; Medjibé, V.; Djomo, A.; Kondaoulé, J.; Rossi, V.; Ngomanda, A.; Maïdou, H. Analyzing Accuracy of the Power Functions for Modeling

Aboveground Biomass Prediction in Congo Basin Tropical Forests. *Open J. For.* **2017**, *07* (04), 388–402. https://doi.org/10.4236/ojf.2017.74023.
186. Kumar, L.; Sinha, P.; Taylor, S.; Alqurashi, A. F. Review of the Use of Remote Sensing for Biomass Estimation to Support Renewable Energy Generation. *J. Appl. Remote Sens.* **2015**, *9* (1), 097696. https://doi.org/10.1117/1.jrs.9.097696.
187. Lee Maynard, C.; Lawrence, R. L.; Nielsen, G. A.; Decker, G. Modeling Vegetation Amount Using Bandwise Regression and Ecological Site Descriptions as an Alternative to Vegetation Indices. *GIScience Remote Sens.* **2007**, *44* (1), 68–81. https://doi.org/10.2747/1548-1603.44.1.68.
188. Kankare, V.; Vastaranta, M.; Holopainen, M.; Räty, M.; Yu, X.; Hyyppä, J.; Hyyppä, H.; Alho, P.; Viitala, R. Retrieval of Forest Aboveground Biomass and Stem Volume with Airborne Scanning LiDAR. *Remote Sens.* **2013**, *5* (5), 2257–2274. https://doi.org/10.3390/rs5052257.
189. Robinson, C.; Saatchi, S.; Neumann, M.; Gillespie, T. Impacts of Spatial Variability on Aboveground Biomass Estimation from L-Band Radar in a Temperate Forest. *Remote Sens.* **2013**, *5* (3), 1001–1023. https://doi.org/10.3390/rs5031001.
190. Zheng, D.; Rademacher, J.; Chen, J.; Crow, T.; Bresee, M.; Le Moine, J.; Ryu, S. R. Estimating Aboveground Biomass Using Landsat 7 ETM+ Data across a Managed Landscape in Northern Wisconsin, USA. *Remote Sens. Environ.* **2004**, *93* (3), 402–411. https://doi.org/10.1016/j.rse.2004.08.008.
191. Coulibaly, L.; Migolet, P.; Adegbidi, H. G.; Fournier, R.; Hervet, E. Mapping Aboveground Forest Biomass from Ikonos Satellite Image and Multi-Source Geospatial Data Using Neural Networks and a Kriging Interpolation. In *International Geoscience and Remote Sensing Symposium (IGARSS)*; 2008; Vol. 3. https://doi.org/10.1109/IGARSS.2008.4779342.
192. Castel, T.; Guerra, F.; Caraglio, Y.; Houllier, F. Retrieval Biomass of a Large Venezuelan Pine Plantation Using JERS-1 SAR Data. Analysis of Forest Structure Impact on Radar Signature. *Remote Sens. Environ.* **2002**, *79* (1), 30–41. https://doi.org/10.1016/S0034-4257(01)00236-X.
193. Wijaya, A.; Gloaguen, R. Fusion of ALOS Palsar and Landsat ETM Data for Land Cover Classification and Biomass Modeling Using Non-Linear Methods. In *International Geoscience and Remote Sensing Symposium (IGARSS)*; 2009; Vol. 3. https://doi.org/10.1109/IGARSS.2009.5417824.
194. Goslee, K.; Walker, S. M.; Grais, A.; Murray, L.; Casarim, F.; Brown, S. Leaf Technicial Guidance Series for the Development of a Forest Carbon Monitoring System for REDD+: Module C-CS: Calculations for Estimating Carbon Stocks. *2010*.
195. biomass, B. S. E. And Biomass Change of Tropical Forests: A Primer. *Rome FAO For. Pap.* **1986**, *134*.
196. Losi, C. J.; Siccama, T. G.; Condit, R.; JE., M. Analysis of Alternative Methods for Estimating Carbon Stock in Young Tropical Plantatiions. *For. Ecol. Manage. 2003* (184), 355–368.
197. Vashum, K. T.; Jayakumar, S. Methods to Estimate Above-Ground Biomass and Carbon Stock in Natural Forests-a Review. *J. Ecosyst. Ecography* **2012**, *2* (4), 1–7.
198. Whittaker, R. H.; GE., L. Carbon in the Biota. In *Woodwell GM, Pecan EV, Carbon*

in the biosphere, Proceedings of the 24th Brookhaven Symposium in biology. Upton, : United States Atomic Energy Commission,1973,. [CrossRef]; pp 281–302.
199. Statistics, F. A. O. Food and Agriculture Organization of the United Nations. *Retrieved* **2010**, *3* (13), 2012.
200. Vicharnakorn, P.; Shrestha, R. P.; Nagai, M.; Salam, A. P.; Kiratiprayoon, S. Carbon Stock Assessment Using Remote Sensing and Forest Inventory Data in Savannakhet, Lao PDR. *Remote SensingJun;* **2014**, *6* (6), 5452–5479.
201. Panel, I. *On Climate Change (IPCC)*; Cambridge University Press: Cambridge, 2007.
202. Rahetlah, B. V; Salgado, P.; Andrianarisoa, B.; Tillard, E.; Razafindrazaka, H.; Le Mezo, L.; VL., R. *Relationship between Normalized Difference Vegetation Index (NDVI) and Forage Biomass Yield in the Vakinankaratra Region*; Madagascar. [Google Scholar] [CrossRef].
203. Goswami, S.; Gamon, J.; Vargas, S.; of Ndvi, T. C. R. Biomass, and Leaf Area Index (LAI) for Six Key Plant Species in Barrow, Alaska. *PeerJ Prepr.* **2015**, *19*.
204. Coelho, A. P.; Rosalen, D. L.; RT., F. Vegetation Indices in the Prediction of Biomass and Grain Yield of White Oat under Irrigation Levels. *Pesqui. Agropecuária Trop.* **2018**, *48* (2), 109–117.
205. Jung, M. *LecoS-A QGIS Plugin for Automated Landscape Ecology Analysis*; 2013.
206. San-Miguel-Ayanz, J.; de Rigo, D.; Caudullo, G.; Houston, D. T.; (Eds.), M. A. European Atlas of Forest Tree Species Publication Office of the European Union, Luxembourg. *2016*.
207. Zecchin, B.; Caudullo, G.; de Rigo, D. Acer Campestre in Europe: Distribution, Habitat, Usage and Threats In: San-Miguel-Ayanz J., de Rigo D., Caudullo G., Houston D. In *T*; Mauri, A., Ed.; European Atlas of Forest Tree Species. Publ. Off. EU: Luxembourg pp. e012c65+, 2016.
208. Eaton, E.; Caudullo, G.; Oliveira, S.; de Rigo D. Quercus robur. And Quercus Petraea in Europe: Distribution, Habitat, Usage and Threats In: San-Miguel-Ayanz J., de Rigo D., Caudullo G., Houston D. In *T*; Mauri, A., Ed.; European Atlas of Forest Tree Species Publ. Off. EU: Luxembourg pp. e01c6df+, 2016.
209. de Rigo, D.; Enescu, C. M.; Houston, D. T.; Caudullo, G. Populus Nigra in Europe: Distribution, Habitat, Usage and Threats In: SanMiguel-Ayanz J., de Rigo D., Caudullo G., Houston D. In *T*; Mauri, A., Ed.; European Atlas of Forest Tree Species Publ. Off. EU: Luxembourg pp. e0182a4+, 2016.
210. Balboa-Murias, M. A.; Rojo, A.; Álvarez, J. G.; Merino, A. Carbon and Nutrient Stocks in Mature Quercus Robur L. Stands in NW Spain. In *Annals of Forest Science*; 2006; Vol. 63, pp 557–565. https://doi.org/10.1051/forest:2006038.
211. Hjelm, B.; Mola-Yudego, B.; Dimitriou, I.; Johansson, T. Diameter--Height Models for Fast-Growing Poplar Plantations on Agricultural Land in Sweden BioEnergy Research. **2015**, *8*, 1759–1768.
212. Helldén, U. A Test of Landsat-2 Imagery and Digital Data for Thematic Mapping Illustrated by an Environmental Study in Northern Kenya, Lund University. *Nat. Geogr. Inst. Rep. No. 47* **1980**.
213. Matikainen, L.; Karila, K. Segment-Based Land Cover Mapping of a Suburban Area—Comparison of High-Resolution Remotely Sensed Datasets Using Classification Trees and Test Field Points. *Remote Sens.* **2011**, *3* (8), 1777–1804.

214. Cohen, J. Weighted Kappa: Nominal Scale Agreement Provision for Scaled Disagreement or Partial Credit. *Psychol. Bull.* **1968**, *70* (4), 213.
215. Banko, G. A Review of Assessing the Accuracy of Classifications of Remotely Sensed Data and of Methods Including Remote Sensing Data in Forest Inventory. **1998**.
216. Russo, A.; Escobedo, F. J.; Timilsina, N.; Schmitt, A. O.; Varela, S.; Zerbe, S. Assessing Urban Tree Carbon Storage and Sequestration in Bolzano, Italy. *Int. J. Biodivers. Sci. Ecosyst. Serv. Manag.* **2014**, *10* (1), 54–70. https://doi.org/10.1080/21513732.2013.873822.
217. Trees and shrubs hardy in the British Isles. Vol. IV. Ri-Z. https://www.cabdirect.org/cabdirect/abstract/19800666681 (accessed May 4, 2020).
218. Jacobs. Annual Report, 2018.
219. Laliberte, A.; Koppa, J.; Fredrickson, E.; Rango, A. Comparison of Nearest Neighbor and Rule-Based Decision Tree Classification in an Object-Oriented Environment. In *2006 IEEE International Symposium on Geoscience and Remote Sensing*; 2006; pp 3923–3926. https://doi.org/10.1109/IGARSS.2006.1006.
220. Chavan, B. L.; Rasal, G. B. Sequestered Standing Carbon Stock in Selective Tree Species Grown in University Campus at Aurangabad , Maharashtra ,. **2000**, *2* (7), 3003–3007.
221. Kumar, L.; Mutanga, O. Remote Sensing of Above-Ground Biomass. Multidisciplinary Digital Publishing Institute 2017.
222. Zhou, W.; Cadenasso, M.; Schwarz, K.; Pickett, S. Quantifying Spatial Heterogeneity in Urban Landscapes: Integrating Visual Interpretation and Object-Based Classification. *Remote Sens.* **2014**, *6* (4), 3369–3386. https://doi.org/10.3390/rs6043369.
223. Cadenasso, M. L.; Pickett, S. T. A.; McGrath, B.; Marshall, V. Ecological Heterogeneity in Urban Ecosystems: Reconceptualized Land Cover Models as a Bridge to Urban Design; Springer, Dordrecht, 2013; pp 107–129. https://doi.org/10.1007/978-94-007-5341-9_6.
224. Band, L. E.; Cadenasso, M. L.; Grimmond, C. S.; Grove, J. M.; Pickett, S. T. A. Heterogeneity in Urban Ecosystems: Patterns and Process. In *Ecosystem Function in Heterogeneous Landscapes*; Springer New York, 2007; pp 257–278. https://doi.org/10.1007/0-387-24091-8_13.
225. Houghton, R. A.; House, J. I.; Pongratz, J.; van der Werf, G. R.; DeFries, R. S.; Hansen, M. C.; Le Quéré, C.; Ramankutty, N. Carbon Emissions from Land Use and Land-Cover Change. *Biogeosciences* **2012**, *9* (12), 5125–5142. https://doi.org/10.5194/bg-9-5125-2012.
226. Houghton, R. A. Aboveground Forest Biomass and the Global Carbon Balance. *Glob. Chang. Biol.* **2005**, *11* (6), 945–958. https://doi.org/10.1111/j.1365-2486.2005.00955.x.
227. Hurtt, G.; Zhao, M.; Sahajpal, R.; Armstrong, A.; Birdsey, R.; Campbell, E.; Dolan, K.; Dubayah, R.; Fisk, J. P.; Flanagan, S.; et al. Beyond MRV: High-Resolution Forest Carbon Modeling for Climate Mitigation Planning over Maryland, USA. *Environ. Res. Lett.* **2019**, *14* (4), 045013. https://doi.org/10.1088/1748-9326/ab0bbe.
228. Hurtt, G. C.; Fisk, J.; Thomas, R. Q.; Dubayah, R.; Moorcroft, P. R.; Shugart, H. H.

Linking Models and Data on Vegetation Structure. *J. Geophys. Res. Biogeosciences* **2010**, *115* (G2), n/a-n/a. https://doi.org/10.1029/2009jg000937.
229. Gu, H.; Williams, C. A.; Ghimire, B.; Zhao, F.; Huang, C. High-Resolution Mapping of Time since Disturbance and Forest Carbon Flux from Remote Sensing and Inventory Data to Assess Harvest, Fire, and Beetle Disturbance Legacies in the Pacific Northwest. *Biogeosciences* **2016**, *13* (22), 6321–6337. https://doi.org/10.5194/bg-13-6321-2016.
230. Huang, W.; Dolan, K.; Swatantran, A.; Johnson, K.; Tang, H.; O'Neil-Dunne, J.; Dubayah, R.; Hurtt, G. High-Resolution Mapping of Aboveground Biomass for Forest Carbon Monitoring System in the Tri-State Region of Maryland, Pennsylvania and Delaware, USA. *Environ. Res. Lett.* **2019**, *14* (9), 095002. https://doi.org/10.1088/1748-9326/ab2917.
231. Varhola, A.; Coops, N. C. Estimation of Watershed-Level Distributed Forest Structure Metrics Relevant to Hydrologic Modeling Using LiDAR and Landsat. *J. Hydrol.* **2013**, *487*, 70–86. https://doi.org/10.1016/j.jhydrol.2013.02.032.
232. Simonson, W. D.; Allen, H. D.; Coomes, D. A. Applications of Airborne Lidar for the Assessment of Animal Species Diversity. *Methods Ecol. Evol.* **2014**, *5* (8), 719–729. https://doi.org/10.1111/2041-210X.12219.
233. Goodwin, N. R.; Coops, N. C.; Tooke, T. R.; Christen, A.; Voogt, J. A. Characterizing Urban Surface Cover and Structure with Airborne Lidar Technology. *Can. J. Remote Sens.* **2009**, *35* (3), 297–309. https://doi.org/10.5589/m09-015.
234. Alonzo, M.; Bookhagen, B.; McFadden, J. P.; Sun, A.; Roberts, D. A. Mapping Urban Forest Leaf Area Index with Airborne Lidar Using Penetration Metrics and Allometry. *Remote Sens. Environ.* **2015**, *162*, 141–153. https://doi.org/10.1016/j.rse.2015.02.025.
235. Shrestha, R.; Wynne, R. H. Estimating Biophysical Parameters of Individual Trees in an Urban Environment Using Small Footprint Discrete-Return Imaging Lidar. *Remote Sens.* **2012**, *4* (2), 484–508. https://doi.org/10.3390/rs4020484.
236. Raciti, S. M.; Hutyra, L. R.; Newell, J. D. Mapping Carbon Storage in Urban Trees with Multi-Source Remote Sensing Data: Relationships between Biomass, Land Use, and Demographics in Boston Neighborhoods. *Sci. Total Environ.* **2014**, *500–501*, 72–83. https://doi.org/10.1016/j.scitotenv.2014.08.070.
237. Jones, T. G.; Coops, N. C.; Sharma, T. Assessing the Utility of Airborne Hyperspectral and LiDAR Data for Species Distribution Mapping in the Coastal Pacific Northwest, Canada. *Remote Sens. Environ.* **2010**, *114* (12), 2841–2852. https://doi.org/10.1016/j.rse.2010.07.002.
238. Fassnacht, F. E.; Latifi, H.; Stereńczak, K.; Modzelewska, A.; Lefsky, M.; Waser, L. T.; Straub, C.; Ghosh, A. Review of Studies on Tree Species Classification from Remotely Sensed Data. *Remote Sens* **2016**, *186*, 64–87.
239. Ørka, H. O.; Hauglin, M. Use of Remote Sensing for Mapping of Non-Native Conifer Species. *76* **2016**.
240. Green Structure and Urban Planning - Final Report https://www.cost.eu/publications/green-structure-and-urban-planning-final-report/ (accessed Aug 17, 2020).
241. Sturiale, L.; Scuderi, A. The Role of Green Infrastructures in Urban Planning for

Climate Change Adaptation. *Climate* **2019**, *7* (10), 119.

Appendix A.

Abbreviations

AGB = Above Ground Biomass

AM = Agisoft Metashape

CCCI = Canopy Content Chlorophyll Index

CHM = Crown Height Model

CS = Carbon Stock

DBH = Diameter at Breast Height

ES = Ecosystem Services

GLCM = Grey Level Co-occurrence Matrix

NDRE = Normalized Difference Red Edge index

NDVI = Normalized Difference Vegetation Index

OBIA = Object-Based Image Analysis

OA = Overall Accuracy

PCA = Principal Component Analysis

RS = Remote Sensing

SfM = Structure-form-Motion